

Optimizing Heat Alert Issuance with Reinforcement Learning

Ellen M. Considine

ELLEN_CONSIDINE@G.HARVARD.EDU

*Department of Biostatistics
Harvard T.H. Chan School of Public Health
Boston, MA 02115, USA*

Rachel C. Nethery

RNETHERY@HSPH.HARVARD.EDU

*Department of Biostatistics
Harvard T.H. Chan School of Public Health
Boston, MA 02115, USA*

Gregory A. Wellenius

WELLENIOUS@BU.EDU

*Department of Environmental Health
Boston University School of Public Health
Boston, MA 02118, USA*

Francesca Dominici

FDOMINIC@HSPH.HARVARD.EDU

*Department of Biostatistics
Harvard T.H. Chan School of Public Health
Boston, MA 02115, USA*

Mauricio Tec

MAURICIOGTEC@HSPH.HARVARD.EDU

*Department of Biostatistics
Harvard T.H. Chan School of Public Health
Boston, MA 02115, USA*

Abstract

A key strategy in societal adaptation to climate change is the use of alert systems to reduce the adverse health impacts of extreme heat events by prompting preventative action. In this work, we investigate reinforcement learning (RL) as a tool to optimize the effectiveness of such systems. Our contributions are threefold. First, we introduce a novel RL environment enabling the evaluation of the effectiveness of heat alert policies to reduce heat-related hospitalizations. The rewards model is trained from a comprehensive dataset of historical weather, Medicare health records, and socioeconomic/geographic features. We use variational Bayesian techniques to address low-signal effects and spatial heterogeneity, which are commonly encountered in climate & health settings. The transition model incorporates real historical weather patterns enriched by a data augmentation mechanism based on climate region similarity. Second, we use this environment to evaluate standard RL algorithms in the context of heat alert issuance. Our analysis shows that policy constraints are needed to improve the initially poor performance of RL. Lastly, a post hoc contrastive analysis provides insight into scenarios where our modified heat alert-RL policies yield significant gains/losses over the current National Weather Service alert policy in the United States.

Keywords: reinforcement learning, climate change, public health, Bayesian modeling, environment

1 Introduction

Extensive evidence links exposure to extreme heat to increases in morbidity and mortality (Ebi et al., 2021). Heat alerts are a practical and low-cost intervention to mitigate these effects (Ebi et al., 2004) by encouraging protective measures such as hydrating more, avoiding physical exertion outdoors, and opening cooling centers. However, studies investigating the effectiveness of heat alerts have observed mixed results (Weinberger et al., 2018; Wu et al., 2023). Developing methods to optimize the issuance of heat alerts to minimize the adverse health impacts of extreme heat is an open problem.

Various challenges stand in the way of solving this problem. First, issuing too many heat alerts may lead to alert fatigue (Nahum-Shani et al., 2017) and health-protective resource depletion on both individual and community/institutional levels. Sequential decision-making (SDM) methods offer a promising yet unexplored avenue for tackling this issue. Second, despite representing a significant health threat on the population scale, local health impacts of heat—and therefore heat alerts—are small and easily confounded in observational data sets (Weinberger et al., 2021). Rare events and low signal (small effects) have been shown to challenge algorithmic decision-making (Frank et al., 2008; Romoff et al., 2018). Third, mainstream SDM methods are not suitable for spatially heterogeneous settings in which a single policy is not equally effective in all regions or dynamically changing contexts (Padakandla, 2021). However, attempting to identify independent policies for each location drastically reduces the amount of available historical data.

In this paper, we lay the foundation for addressing these challenges by introducing a framework for optimizing heat alert issuance using reinforcement learning (RL) enabled by statistical modeling. The RL paradigm enables learning SDM policies that indicate whether to issue a heat alert at each point in time with the goal of minimizing health risk—which in RL terms is the negative reward signal—over the long run. The two main components of our framework are visualized in Figure 1 and summarized below.

First, we create a realistically challenging SDM environment for heat alert issuance, structured as a Markov Decision Process (MDP) under a budget constraint. Key components of the dataset used to create this environment are heat alerts issued by the U.S. National Weather Service (NWS) from 2006–2016, hospitalization records from Medicare, ambient heat index, and other covariates informed by the epidemiological literature. To estimate the rewards under both observed (NWS) and counterfactual alert policies, we fit a statistical model of hospitalizations that allows for spatiotemporal heterogeneity, uncertainty quantification, and fast inference using variational Bayes (Tzikas et al., 2008). For the state-transition model, we exploit a factorization of the state space into an endogenous component with known transition dynamics and an exogenous component sourced from observed weather trajectories. This use of real data allows us to make grounded inferences about the effectiveness of both observed and counterfactual heat alert policies in the U.S. We call our overall approach to creating the environment Bayesian Rewards Over Actual Climate History (BROACH), because it broaches development of SDM for heat alerts and other climate & health problems.

Second, we use our environment to train RL models and then to evaluate the RL policies as well as the NWS and alternative baseline policies—all subject to the same alert budget for comparison. Our evaluation identifies issues during training that lead to poor performance of

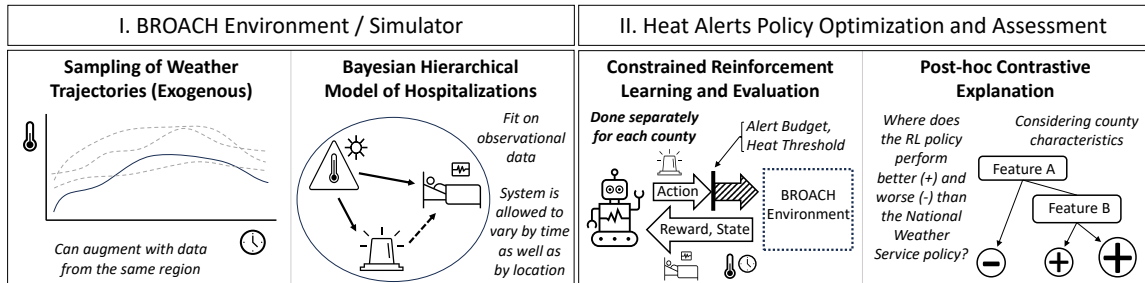


Figure 1: Overview of the heat alerts RL framework.

standard, widely-used RL algorithms. We address these issues by introducing conceptually simple modifications which enable learning of policies that reduce hospitalizations relative to the NWS policy. These modifications include restricting the RL model to issue alerts only on extremely hot days and optimizing policies for each location separately. Lastly, we perform contrastive explanation (van der Waa et al., 2018; Narayanan et al., 2022) of the RL policies by comparing their attributes (e.g., how often does the policy issue alerts on consecutive days) within and across locations to those of the NWS and alternative baseline policies. Specifically, we use visualizations and Classification and Regression Trees (CART) to illustrate systematic differences between these policies and identify characteristics of locations where RL-based policies might offer the greatest improvements in public health.

Contributions to RL Our heat alerts environment will be made publicly available in an open-source Python package compatible with the Gymnasium framework for RL (Towers et al., 2023). This challenging, data-driven environment can be used as a benchmark. The relatively poor performance of standard widely-used RL algorithms indicates the need for developing new general-purpose RL algorithms that perform robustly in this setting. Further, our methodology to create the environment harnessing real data can be used as a blueprint for other data-driven RL simulators, particularly for problems with exogenous state space components and multiple individuals or locations.

Contributions to climate change adaptation This work makes progress towards the ultimate goal of deploying data-driven policies in the real world to protect public health from extreme heat events by training and evaluating RL policies in an environment that is realistic in terms of both weather patterns and the relationships between heat exposure, heat alerts, and hospitalizations. Broadly, our development of an RL/SDM workflow for heat alert optimization and our identification of both strengths and weaknesses of RL in this context paves the way for future research on this problem. Our methodological approach can also be harnessed to optimize alert policies for other kinds of events projected to increase in severity or frequency due to climate change, such as wildfire smoke or extreme cold days.

2 Related work

Heat alert optimization Recent approaches to improving the issuance of heat alerts include (i) the development of a causal inference technique for stochastic interventions to infer whether increasing the probability of issuing a heat alert would be beneficial (Wu et al., 2023) and (ii) a comparison of methods to identify optimal thresholds above which heat

alerts should always be issued (Massetot et al., 2021). Crucially, neither of these approaches addresses the complications of sequential dependence, i.e., the potential for alert fatigue and running out of resources to deploy precautionary measures. To our knowledge, SDM techniques have not yet been explored in a climate & health setting.

RL with exogenous states Several recent papers utilize a decomposition of the state space into exogenous vs. endogenous components, but none of these methods apply directly in the heat alerts setting. Efroni et al. (2022) provide theoretical analysis and guarantees for sample efficiency in tabular (finite state) environments with an unknown subset of exogenous variables. Sinclair et al. (2023) introduce “hindsight learning” for situations where a known reward function and an exact solver under a fixed exogenous trajectory are available. Lee et al. (2023) also use hindsight, but do so in the context of identifying latent states within a partially observable MDP. (While the alert fatigue of the populace might be considered a latent aspect of each state, it isn’t observable in hindsight either.)

Statistical modeling for RL environments Using a statistical model for the reward function in an RL environment is common practice in settings with empirical data. Bayesian models in particular have been used to identify the effect of intervention in health-related applications and dynamic treatment regimes (Liao et al., 2020; Tec et al., 2023; Zajonc, 2012). For spatiotemporal or otherwise heterogeneous environments, previous studies have also used a combination of local modeling and global modeling that takes into account the spatial or hierarchical structure to create simulated environments for RL (Wu et al., 2021; Li et al., 2018; Agarwal et al., 2021).

Constrained learning The use of domain knowledge-based policy restrictions in RL has been found to speed up learning and to guide the learned policy in pragmatic directions (Mu et al., 2021). This supports our restriction of RL heat alerts to very hot days. More generally, incorporating “cost” or “safety” constraints is of interest for many RL applications (Laber et al., 2018; Carrara et al., 2019). A common approach in the constrained RL literature is to use Lagrange multipliers (Guin and Bhatnagar, 2023; Ray et al., 2019), however, these methods do not enforce a strict constraint/budget. To enable direct comparison with the observed NWS policy, we impose a strict alert budget, which can be viewed as a simplified variation of the indicator approach formulated by Xu et al. (2022). An alternative approach to handling both the alert budget and restriction of alerts to very hot days would be to model the extent of distributional overlap with the observed NWS policy, and penalize actions that have too little overlap (Xu et al., 2022). However, our approach has the benefit of being relatively interpretable.

Contrastive policy explanations Another important swath of literature surrounds post-hoc explainability in RL (Heuillet et al., 2021). Contrastive analysis has been used to explain differences between RL policies and more familiar / intuitive policies (van der Waa et al., 2018; Narayanan et al., 2022). We note that while CART has been used to try and mimic RL policies (Puiutta and Veith, 2020), our use of it to analyze differences between policies has not been previously documented.

3 Problem Setup: Heat Alerts as a Sequential Decision-Making Process

RL methods typically operate within the framework of Markov Decision Processes (MDPs) (Sutton and Barto, 2018). We provide some technical background and then describe how we apply this framework to the heat alerts problem.

3.1 Background on MDPs

An infinite-horizon MDP is defined as a tuple $\mathcal{M} = \langle S, A, R, P, d_0, \gamma \rangle$, where S denotes the set of states, A represents the available actions, $R : S \times A \rightarrow \mathbb{R}$ is the expected reward function, $P : S \times A \rightarrow \Delta(S)$ is the transition function¹, $d_0 : S \rightarrow \Delta(S)$ is the initial state distribution, and $0 < \gamma < 1$ is the time discount factor. A policy $\pi : S \rightarrow \Delta(A)$ is a mapping from states to probability distributions over actions. The state value function of π is $V^\pi(s) := \mathbb{E}_\pi[\sum_{t=0}^{\infty} \gamma^t R(s_t, a_t) | s_0 = s]$ and the state-action value function is $Q^\pi(s, a) := R(s, a) + \gamma \mathbb{E}_{s' \sim P(s, a)}[V^\pi(s')]$. The policy optimization goal is to identify π^* that maximizes the expected cumulative reward, also known as the *objective*

$$J(\pi) := \mathbb{E}_{s_0 \sim d_0}[V^\pi(s_0)]. \quad (1)$$

Under regularity conditions (Puterman, 2014; Bertsekas and Shreve, 1996), the optimal policy is deterministic and is the unique solution (up to tie-breakers) of the Bellman optimality equation

$$Q^*(s, a) = R(s, a) + \gamma \mathbb{E}_{s' \sim P(s, a)}[\max_{a'} Q^*(s', a')], \quad (2)$$

where Q^* denotes the state-action value function of π^* . The optimal action is recovered deterministically by $\pi^*(s) = \arg \max_a Q^*(s, a)$.

These definitions can be adapted for the case when the decision process has a finite horizon H , which is known as the finite-horizon or “episodic” MDP setting. A (non-stationary) policy is defined as a collection of decision rules $\pi = \{\pi_t : S \rightarrow \Delta(A)\}_{t=0}^{H-1}$. The value function is defined for each time step as $V_t^\pi(s) = \mathbb{E}_\pi[\sum_{h=t}^{H-1} \gamma^{h-t} R(s_h, a_h) | s_t = s]$. The policy optimization goal is to find π^* maximizing $J(\pi) := \mathbb{E}_{s_0 \sim d_0}[V_0^\pi(s_0)]$. It is typical to consider γ equal or close to one. A finite-horizon MDP can be cast as an infinite-horizon MDP by considering the end of the episode to be an absorbing state generating zero rewards and including t as part of the state vector s_t to ensure the Markov property (Sutton and Barto, 2018).

RL algorithms search for the optimal policy of an MDP by interacting with an environment that generates rewards and transitions, where the RL does not possess knowledge of the reward and transition functions (Sutton and Barto, 2018).

3.2 Issuing Heat Alerts as a Constrained MDP

We now describe the MDP components associated with the heat alert optimization problem, summarized in Table 1. Each MDP \mathcal{M}_k corresponds to a geographic area $k \in \mathcal{K}$, and episodes are indexed as $j \in \mathcal{J}$. In this work, geographic areas are U.S. counties, and each episode spans the warm season from May 1st to September 30th of a specific year. The horizon or length of the episode is $H = 152$ days. State-action-reward triples are denoted

¹ $\Delta(\cdot)$ denotes the set of probability distributions over the set “.”.

RL Term	Notation	Meaning in the Heat Alerts Application
episode	$t \in \{0, \dots, H - 1\}$	the $H = 152$ days of the warm season/summer in a specific year and county; H is the horizon
state	$s_t = (\xi_t, x_t)$	a vector of time-varying factors influencing the effect of heat on hospitalizations and the effectiveness of an alert; ξ_t is the exogenous component (e.g., heat index) and x_t is the endogenous component (e.g., history of heat alerts)
action	a_t	whether a heat alert is issued (1) or not (0) at time t
reward	$r_t = R(s_t, a_t)$	daily rate of heat-related hospitalizations at time t ; a negative sign transform is applied so that fewer hospitalizations corresponds to a greater reward
agent	—	the algorithmic decision-maker that implements a policy to determine when to issue heat alerts
policy	$\pi(a_t s_t)$	the heat alert issuance rule; the NWS policy is the rule that was used to issue heat alerts in the U.S. from 2006-2016
cumulative reward / return	$\sum_{h=t}^{H-1} r_h$	sum of remaining reward (transformed hospitalizations); unless otherwise specified, “cumulative” implies $t = 0$
intervention / alert budget	$\sum_{t=0}^{H-1} a_t \leq b$	the maximum number of heat alerts that can be issued in a given county-summer; in our experiments, the observed number of NWS alerts

Table 1: MDP/RL terminology in the context of the heat alerts environment.

$(s_t^{(k,j)}, a_t^{(k,j)}, r_t^{(k,j)})$. The index (k, j) is omitted when the context is clear. Warm seasons are also referred to as “summers” for brevity.

The action a_t on day t is either 1 (issue a heat alert) or 0 (do not issue a heat alert). As introduced in Section 1, when issuing alerts, we must be wary of alert fatigue: both individuals and communities likely have diminished will and resources to respond to any single alert as more alerts are issued. We adopt a strict action budget-constrained approach, optimizing the policy subject to $\sum_{t=0}^{H-1} a_t \leq b$. In our experiments, to directly compare counterfactual alert policies with the NWS policy, we fix b to the number of heat alerts that the NWS issued in any given county-summer.

The reward $r_t = R(s_t, a_t)$ is the expected rate of heat-related hospitalizations at time t , transformed such that fewer hospitalizations correspond to a greater reward. Specifically, if $\rho_t(a)$ represents the *per capita* rate of heat-related hospitalizations on day t when action $a \in \{0, 1\}$ is taken², then the reward r_t is proportional to $-\mathbb{E}[\rho_t(a_t)|s_t]$.

The state vector s_t contains the factors underlying the effect of heat on hospitalizations and the effectiveness of heat alerts at reducing hospitalizations. It can be decomposed as $s_t = (\xi_t, x_t)$, where ξ_t is the exogenous component and x_t is the endogenous component. The exogenous component is defined as the portion of the state space that is not influenced by the agent’s actions a_t . It consists of the heat index (weather) data and temporal characteristics such as the day of the summer and an indicator for weekend status. The endogenous component x_t includes the number of heat alerts issued in the recent past as well as the remaining alert budget for that summer. The transition function of the endogenous

²The notation $\rho_t(a)$ here is borrowed from the causal inference literature to denote counterfactuals (Rubin, 2005).

component is known and deterministic. Hence, the full state transition function admits a factorization

$$P(s_{t+1}|s_t, a_t) = P((\xi_{t+1}, x_{t+1})|(\xi_t, x_t), a_t) = P_\xi(\xi_{t+1}|\xi_t)P_x(x_{t+1}|x_t, a_t) \quad (3)$$

where P_x is deterministic. Details on the state space and the exogenous-endogenous decomposition used to create our RL environment are provided in Section 4.

4 The RL Environment

RL requires an interactive environment that generates transitions between states and rewards in response to the actions taken in each state. We create such an environment with the following design objectives:

1. The environment must allow the evaluation of general-purpose RL algorithms.
2. It must be grounded in real data to permit inferences about the effectiveness of different heat alert policies in the U.S.
3. It must deal with the low signal that characterizes the health effects of heat and heat alerts as well as the heterogeneity of these relationships across space and time.

We present Bayesian Rewards Over Actual Climate History (BROACH), a methodology that meets these objectives. This section is organized as follows. First, we provide an overview of the data sources used to learn the components of the environment, providing additional details in Appendix A. Next, we describe the state space of the decision process, the reward function, the alert budget implementation, and the transition function. While this approach is explained in the context of heat alerts, it can easily be generalized to other types of climate-related exposures and interventions.

4.1 Data Sources

Heat alerts and heat index We use the dataset of Weinberger et al. (2021) with daily, county-level records of the heat alerts issued by the NWS in the summers of 2006–2016, as well as the heat index, which is a measure of the combined effect of temperature and humidity on the human body. We consider the 761 counties with a population greater than 65,000 to avoid locations with very few hospitalizations and to focus on the most populous areas. Figure 2 shows the counties considered, which account for approximately 75% of the population and 25% of the number of counties.

To understand the observed heat alert data, note that while the decision to issue an alert is based on temperature thresholds (differing in northern and southern states), it is also strongly affected by the discretion of the local office (Hawkins et al., 2017). Analysis by Hondula et al. (2022) suggests that spatial variability in the current NWS/local office approach is not well aligned with the health risk from heat. However, the stochasticity induced by local discretion provides an opportunity to study and improve the health protectiveness of heat alerts (Wu et al., 2023).

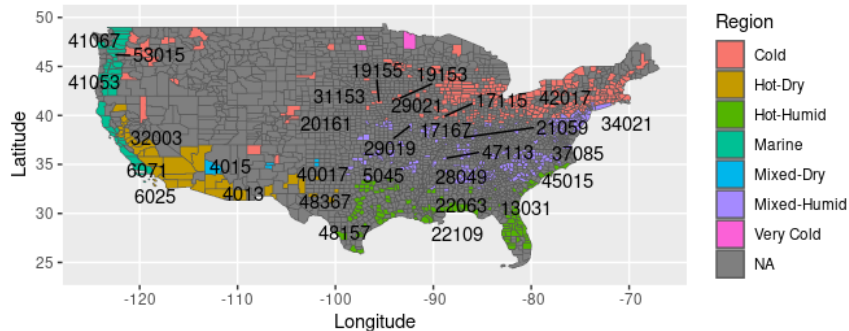


Figure 2: Map of the counties considered and their regional climate zone classifications. All the colored counties are used in the Bayesian rewards model and RL environment; the 30 counties with annotated FIPS codes are used in the RL experiments.

Heat-related hospitalizations We merged the heat alert and weather data with daily, county-level hospitalization counts from the Centers for Medicare and Medicaid Services (CMS). We included cause-specific hospitalizations previously found to be associated with extreme heat in the Medicare population: septicemia, peripheral vascular disease, urinary tract infections, and diabetes mellitus with complications (Bobb et al., 2014). We excluded heat stroke and fluid and electrolyte disorders (which were also found to be associated with extreme heat in Medicare) because Weinberger et al. (2021) observed a positive association between heat alerts and hospitalizations with these causes. They hypothesized it was due to increased awareness of heat-related symptoms and seeking medical care. Figure 3 illustrates this scenario as an unobserved mediation problem (Pearl, 2012), which affects the identification of the preventive effect of heat alerts. We refer to the remaining causes, which we pool together into one outcome variable, as not-obviously heat-related (NOHR) hospitalizations.

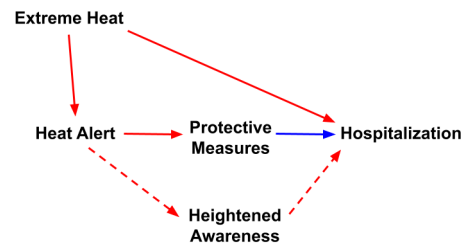


Figure 3: Unobserved mediation of the effect of heat alerts on hospitalizations by heightened awareness.

County-level characteristics Spatial heterogeneity in the effect of heat on hospitalizations and the effectiveness of heat alerts can occur due to people in different regions being affected differently by the same absolute temperatures due to geographical self-selection and climate adaptation, differential health susceptibility and/or individual agency associated with socioeconomic status and population density, and variable response to heat alerts due to local policy and political ideology (Ng et al., 2014; Zanobetti et al., 2013; Errett et al., 2023; Cutler et al., 2018). To characterize this spatial heterogeneity, we compiled county-level estimates of population density and median household income (U.S. Census Bureau, 2014), regional classifications of climate zones (U.S. Energy Information Administration,

Component	Variable
exogenous (ξ_t)	quantile of heat index (QHI), excess heat, day of summer, weekend indicator
endogenous (x_t)	Number of heat alerts issued in the last 14 days, indicator of whether a heat alert was issued yesterday, and the remaining alert budget

Table 2: The state space, decomposed into exogenous and endogenous components.

2020), broadband (internet) usage data (Microsoft AI for Good Research Lab, 2021), presidential election returns (MIT Election Data and Science Lab, 2018), and fine particulate matter (PM_{2.5}) (Hammer et al., 2020). For the latter: there is strong evidence of adverse synergistic health impacts of air pollution and heat (Anenberg et al., 2020).

4.2 The State Space

Table 2 summarizes the variables used in the state space of the MDP. Recall that the state space can be factorized as $s_t = (\xi_t, x_t)$, where ξ_t is the exogenous component and x_t is the endogenous component. The exogenous component contains the quantile value of the day’s observed heat index (QHI)—within each county across warm seasons for all the years. Using the QHI allows us to account for long-term climate adaptation. Note that in addition to alert fatigue, time-varying factors that can modify the effect of heat on hospitalizations and the effectiveness of heat alerts include the relative heat compared to recent days (Heo et al., 2019), and the timing of heat waves within the warm season (Anderson and Bell, 2011). Therefore, the QHI is complemented in our state space by the day of summer and a weekend indicator, as well as an excess heat variable, which we define as the difference between the QHI and the average of the last three days’ QHI, a time window informed by the literature on heat waves and health (Metzger et al., 2010). The endogenous component contains the number of heat alerts issued in the last 14 days, an indicator of whether a heat alert was issued yesterday, and the remaining alert budget for that episode.

4.3 The Reward Function: A Hierarchical Model of Hospitalizations

Using the notation of Section 3.2, let $\rho_t^{(k,j)}(a)$ be the expected *per capita* NOHR hospitalization rate at time t in county-summer (k, j) when taking action a . We propose the following scaled reward function:

$$r_t^{(k,j)}(a) := C_1 - C_2 \rho_t^{(k,j)}(a) \quad (4)$$

where C_1 and C_2 are positive constants. Note that choices of C_1 and C_2 do not change the optimal policy, but can help stabilize learning. We choose $C_1 = 1$ and C_2 as the reciprocal of the observed hospitalization rate through the entire summer.

To learn the expected hospitalization rate/reward, we train a Bayesian hierarchical model with the desiderata of (a) facilitating obtainment of confidence intervals when evaluating RL policies and (b) allowing for spatial heterogeneity in the health effects of heat and heat alerts.

Let $y_t^{(k,j)}(a)$ denote the counterfactual outcome representing the number of NOHR hospitalizations for action $a \in \{0, 1\}$, and $n^{(k,j)}$ denote the total population susceptible to hospitalization in county k in episode j . We introduce two functions—to be learned—governing the counterfactual hospitalization rate at county k as a function of the state. First, $\lambda_k: S \rightarrow \mathbb{R}^+$ denotes the baseline rate of hospitalizations when no alert is issued. Second, $\tau_k: S \rightarrow (0, 1)$ expresses the effectiveness of issuing an alert as a multiplicative reduction factor. The top-level hospitalization model is

$$\begin{aligned} y_t^{(k,j)}(a) &\sim \text{Poisson}(n^{(k,j)} \rho_t^{(k,j)}(a)), \\ \rho_t^{(k,j)}(a) &:= \lambda_k(s_t^{(k,j)})(1 - a \cdot \tau_k(s_t^{(k,j)})), \end{aligned} \tag{5}$$

for all $(k, j) \in \mathcal{K} \times \mathcal{J}$ and $t \in \{0, \dots, H - 1\}$. The Poisson distribution/loss function is the natural choice for count data and recommended for health outcomes data due to its correspondence to the Cox survival model (Cameron and Trivedi, 2013; Austin, 2017). Because $Y \sim \text{Poisson}(\mu)$ implies $\mathbb{E}[Y] = \mu$, it follows that $\rho_t^{(k,j)}(a)$ is the expected per capita hospitalization rate.

The baseline and effectiveness functions Note that λ_k and τ_k are unique to each location k , allowing for spatial heterogeneity and thus reducing the possibility of unobserved spatial confounding (Bell and Jones, 2015; Nobre et al., 2021; Tec et al., 2024). However, this design introduces the challenge of estimating these functions under limited data for each county (11 summers between 2006 and 2016). This challenge is amplified by the low signal in the health effects of heat and heat alerts (Weinberger et al., 2021). To address this, we adopt a (generalized) linear model for λ_k and τ_k paired with (i) borrowing statistical strength across counties using a data-driven random effects prior and (ii) injecting domain knowledge on the signs of certain coefficients. The functions λ_k and τ_k are specified as

$$\begin{aligned} \lambda(s_t^{(k,j)}) &:= \exp\left(\beta_k^\top s_t^{(k,j)}\right), \\ \tau(s_t^{(k,j)}) &:= \text{sigmoid}\left(\delta_k^\top s_t^{(k,j)}\right), \end{aligned} \tag{6}$$

where β_k and δ_k are the model coefficients for each county $k \in \mathcal{K}$. While this specification is a linear combination of state variables, we allow for non-linear effects by using a piecewise linear basis expansion on the quantile of heat index (QHI) and a spline basis on the day of summer. We do not write out these expansions in Equation (6) to avoid clutter.

Figure S3 illustrates the interaction of λ_k and τ_k to capture the total effect of heat alerts on NOHR hospitalizations. For instance, we see that in early summer it is possible to have high heat alert effectiveness even when the heat index is not as high as it is later in the summer, possibly because people are less well-adapted to heat and/or more responsive to heat alerts early on.

Data-driven prior We propose a data-driven prior distribution that allows borrowing statistical strength from other locations while preserving the possibility of spatial heterogeneity. Let w_k denote the vector of county-level features that are not included in the state vector but are predictive of the effect of heat and heat alerts on hospitalizations (see “County-level characteristics” in Section 4.1), and let $\gamma_k = [\beta_k; \delta_k] = (\gamma_k^\ell)_{\ell=1}^L$ denote

the parameters corresponding to county k . Then, the prior distribution of each γ_k^ℓ is set independently as

$$p_\theta(\gamma_k^\ell | \sigma_\ell, w_k) = \begin{cases} \text{Normal}(\gamma_k^\ell; f_\theta(w_k)_\ell, \sigma_\ell^2) & \text{no domain knowledge,} \\ \text{LogNormal}(\gamma_k^\ell; \exp(f_\theta(w_k)_\ell), \sigma_\ell^2) & \text{if } \gamma_k^\ell \in (0, \infty), \\ \text{NegLogNormal}(\gamma_k^\ell; -\exp(f_\theta(w_k)_\ell), \sigma_\ell^2) & \text{if } \gamma_k^\ell \in (-\infty, 0), \end{cases} \quad (7)$$

where f_θ is a feed-forward neural network (with weights θ and L outputs) specifying the prior mean as a function of the spatial features, and σ_ℓ specifies the prior scale. We use a standard hyper-prior $p(\sigma_\ell) = \text{HalfCauchy}(\sigma_\ell)$ (Gelman, 2006).

The domain knowledge constraints we utilize are: (i) past heat alerts cannot increase the baseline hospitalization rate—in other words, alert fatigue can be identified only in τ —and (ii) higher QHI cannot decrease the effectiveness of heat alerts—note that this is conditional on day of summer.

The weights θ are learned from the data to characterize the prior distribution that best describes the latent space according to the data. As remarked in Wang et al. (2019), this procedure can be seen as a form of Empirical Bayes. According to this viewpoint, we can interpret the prior mean function f_θ in Equation (7) as an encoder that maps the county-level features w_k to a data-driven probability distribution over a latent space. The coefficients γ_k are latent variables in this space. The predictive model $\rho_t^{(k,j)}(a)$ in Equation (5) acts as a decoder.

Training Traditional Bayesian inference methods using Markov Chain Monte Carlo are computationally prohibitive for our model due to the high dimensionality of parameters and the number of observations for each county. To address this issue, we use variational inference, which introduces an approximation of the true posterior distribution of the model parameters. We summarize the approach.

Let $(\gamma, \sigma) \sim q_\psi$ denote an approximation of the true posterior distribution where ψ are the learnable parameters of the approximating distribution q_ψ . Next, let $o_t^{(k,j)} = (s_t^{(k,j)}, a_t^{(k,j)}, y_t^{(k,j)}, n^{(k,j)})$ denote a data point in the training set and $\mathcal{L}(o_t^{(k,j)}; \gamma_k)$ be the Poisson log-likelihood corresponding to this data point (see Equation (5)). Variational inference attempts to maximize the likelihood of the observed data while penalizing the divergence between the variational posterior q_ψ and the prior $p_\theta(\gamma, \sigma | w) = \prod_{k,l} p_\theta(\gamma_k^\ell | \sigma_\ell, w_k) \prod_l p(\sigma_\ell)$. The optimization objective is to maximize the evidence lower bound (ELBO) given by

$$\text{ELBO}(\psi, \theta) = \mathbb{E}_{q_\psi} \left[\sum_{k,j,t} \mathcal{L}(o_t^{(k,j)}; \gamma_k) \right] - D_{\text{KL}}(q_\psi(\gamma, \sigma) \| p_\theta(\gamma, \sigma | w)), \quad (8)$$

where D_{KL} denotes the Kullback-Leibler divergence. To ensure the variational posterior is flexible enough to approximate the true posterior, we use a low-rank multivariate normal distribution (Tomczak et al., 2020). This approach uses a bijective transform of the parameters to an unconstrained space and then applies a low-rank factorization to the covariance matrix of the multivariate normal distribution. Thereby, it allows for efficient computation while approximating the true correlation structure of the joint posterior distribution. The data-driven prior parameters θ are learned jointly with the variational parameters ψ using stochastic optimization.

Implementation We fit this model using the Python package Pyro (Harpole et al., 2019). In Appendix B, we confirm the convergence of the ELBO and perform additional experiments to validate the model calibration and predictive performance. These experiments indicate good performance in the uncertainty quantification properties of the model and demonstrate a reasonable fit to the data. Appendix B also notes the neural network architecture of f_θ .

To utilize the rewards model within the BROACH environment, we draw from the variational posterior distribution at the start of each episode of the MDP. This vector of coefficients $\tilde{\gamma}_k$ is then used throughout the episode to calculate $r_t^{(k,j)}$ given $(s_t^{(k,j)}, a_t^{(k,j)})$.

4.4 The Alert Budget

Each episode in our MDP starts with a fixed alert budget b . This can be specified as a constant, sampled from a range of values, or set to be the same as the number of alerts issued by the NWS in that county-summer. As the agent steps through the episode, once $\sum_{h=0}^t a_h = b$, it is prohibited from issuing any more alerts: it can only obtain the reward $\rho_h(0)^{(k,j)}$ for days $h = t, \dots, H - 1$.

4.5 The Transition Function: Observing Actual Weather/Climate History

Equation (3) in Section 3.2 introduced the factorization of the transition function into exogenous (P_ξ) and endogenous (P_x) components. We leverage this decomposition to use real data for the exogenous trajectories, and introduce a data augmentation scheme to avoid overfitting in the context of single-county RL.

Sampling of exogenous trajectories Recall that the endogenous aspect of our state space, heat alert history, is deterministically updating, so does not need to be modeled probabilistically. The key observation in the heat alert setting is that the more complicated aspect of the environment, the weather/climate, also does not need to be modeled because it is completely exogenous to heat alert decision-making. In this setting, developing a model for the weather is not only unnecessary, but would unavoidably introduce error. Instead, we sample real observed weather trajectories.

Regional data augmentation The issue with this approach is that there are only 11 years of exogenous trajectories (2006-2016) available per county during which we also have heat alert data—which is needed when we use observed alert budgets (which are paired with the observed weather) for comparison with the NWS. To mitigate the potential for RL overfitting to these 11 years, we propose data augmentation by sampling weather trajectories from other counties in the same regional climate zone³ (U.S. Energy Information Administration, 2020) during RL training and validation / tuning.

5 Learning and Evaluating Heat Alert Policies with RL

We conduct experiments to (a) assess the ability of standard RL algorithms to learn effective heat alert policies in the BROACH environment, (b) test various modifications to these

³Due to the large size/geographic range of the “Cold” zone, we grouped its counties into eastern and western subsets for the data augmentation sampling.

algorithms, and (c) compare the resulting policies to the NWS policy and other intuitive baselines. We then investigate heterogeneous performance of the RL policies to provide domain-relevant insights.

5.1 Policy Constraint: Alerts Allowed Only on Very Hot Days

Foreshadowing our findings, standard RL algorithms struggle to learn to conserve their alert budgets for later in the summer, resulting in poor performance in the BROACH environment (Table 3). A major modification we implement to encourage more effective behavior is restricting the issuance of heat alerts to days above a QHI threshold, optimized separately for each county. To optimize the QHI threshold, we test the sequence of values between 0.5 and 0.9 (an interval selected to ensure overlap with the NWS policy), by every 0.05, and select the value that yields the best return on our validation set, which is specified in the following section. Names of models including this adaptation have the suffix “.QHI”.

5.2 Experimental Setup

For all training and evaluations, we take the alert budget for each county-summer to be the observed number of alerts issued by the NWS in that county-summer.

RL baselines We investigate the use of four of the most widely used RL algorithms: Deep Q-learning (DQN), Quantile Regression Deep Q-learning (QRDQN), Trust Region Policy Optimization (TRPO), and Advantage Actor-Critic (A2C). We use standard implementations of these methods available in the `Stable-Baselines3` library for Python (Raffin et al., 2021).

To ground our analysis and discussion, we note that DQN and QRDQN are off-policy methods which learn deterministic policies by directly solving for the optimal value function using the Bellman optimality condition in equation 2; exploration is induced only during training, for instance, using the epsilon-greedy algorithm. Whereas, TRPO and A2C are on-policy methods which learn stochastic policies by direct optimization of the expected return in Equation (1) using refinements of the policy gradient theorem (Sutton et al., 1999); exploration is inherent. QRDQN differs from DQN in that rather than estimating the average return from taking action a at state s , it estimates the distribution over the returns using quantile regression. Compared to other common stochastic policy gradient algorithms, TRPO is distinguished by its constraint on the size of the optimization step, so that the new policy lies within a “trust region” from the previous policy, in which local approximations of the policy function are still accurate (Han et al., 2023). A2C improves on the basic setup of actor-critic by updating its policy model using the advantage function, which indicates how much better an action is than the alternative(s), rather than just the state-action value of that one action; this helps increase model stability (Han et al., 2023).

NWS and simple alternative baselines To evaluate each of the RL policies, we compare them to the observed NWS policy as well as several counterfactual baselines: most simplistically, issuing zero alerts, randomly selecting b days (RANDOM) on which to issue alerts, and selecting the b days with the highest QHI that summer (TOPK)—the latter is an oracle policy (not implementable in the real world) because to use it, we would have to know the daily QHI across the whole warm season in advance. We also implement the gen-

eral guidelines that NWS recommends in the absence of local criteria for issuing heat alerts (BASIC.NWS): alert if the heat index is $\geq 100^\circ\text{F}$ in northern states and $\geq 105^\circ\text{F}$ in southern states (Hawkins et al., 2017). Lastly, we implement a policy of always issuing alerts on days above a per-county optimized QHI threshold until the budget runs out (AA.QHI).

Training data The counties for which NWS issued few heat alerts had high-variance estimates of heat alert effectiveness in the rewards model in Section 4. Therefore, for the RL experiments, we chose to only consider counties where at least 75 heat alerts were issued during 2006-2016. This left 170 counties. For computational and analytical purposes, we further subset this to 30 counties spread across the five major climate regions, prioritizing those with higher variance in estimated heat alert effectiveness (indicating a higher signal identified by the rewards model). The FIPS codes of these 30 counties are annotated in Figure 2. Additionally, characteristics of these 30 counties are summarized in Table S2 and details of our selection procedure are provided in Appendix C.1.

Evaluation metric The main metric we use for policy comparison is the average cumulative reward per episode (“average return”). To estimate this metric fairly, we hold three years of data (2007, 2011, and 2015) out of RL training, referred to as the evaluation years. For the purposes of RL hyperparameter tuning (details in Appendix C.2) and selection of the optimal QHI threshold for each county, we consider the regionally augmented weather trajectories and associated heat alert budgets from the evaluation years *excluding the county of interest* to be the validation data set. The final evaluation results (reported in tables and figures) are obtained by drawing 1,000 sets of coefficients from the Bayesian rewards model posterior and calculating the return under each policy with weather and budgets *only from the county of interest* during the evaluation years. These validation/tuning and evaluation procedures are described algorithmically in Appendix D. After calculating the average returns for the 30 counties under each competing policy, we compare each policy’s returns with the associated returns under the observed NWS policy for the same counties using a Wilcoxon-Mann-Whitney test. This nonparametric test allows us to compare the distribution of returns under two different policies, accounting for the fact that the counties (and their associated policies and returns) are highly heterogeneous, so the differences between the policies are not normally distributed.

Sensitivity analysis In the main analysis, we evaluate each county-specific implementation of DQN, QRDQN, TRPO, and A2C by allowing each algorithm to deploy the type of policy that it optimizes during training: deterministic for DQN and QRDQN and stochastic for TRPO and A2C. As a sensitivity analysis, we also deterministically evaluate the TRPO and A2C policies, selecting whichever action has a higher probability under the policy function. The names of these models have the prefix “DET”. In another sensitivity analysis, we investigate whether the RL models can learn to anticipate the general trajectory of weather / subseasonal variation in the warm season by augmenting the RL state space with information about the future. Specifically, we test whether inclusion of the change in heat index over each of the next 10 days, as well as the 50th-100th (by every 10) percentiles of QHI for the remainder of the summer, improves RL performance. In real-time deployments of RL models, this kind of future information would not be known but could be sourced from weather forecasts or climate model projections. Of course, such forecasts / model projec-

Policy	Median Diff.	WMW	P-value	NOHR Hosps Saved vs NWS (vs Zero) Per Summer	
				Median / 10,000 Medicare	Approximate Total
*TOPK	0.022	406	0.0002	0.023 (1.96)	113 (9,603)
RANDOM	-0.015	177	0.88	-0.013 (1.98)	-64 (9,697)
BASIC.NWS	-0.286	30	1.0	-0.283 (1.45)	-1,388 (7,110)
AA.QHI	0.03	348	0.0025	0.029 (1.99)	143 (9,747)
DQN	-0.123	43	0.99995	-0.102 (1.83)	-502 (8,989)
QRDQN	-0.117	51	0.99991	-0.098 (1.85)	-480 (9,046)
TRPO	-0.065	97	0.99742	-0.063 (1.9)	-309 (9,321)
A2C	-0.063	100	0.99689	-0.062 (1.9)	-301 (9,317)
DQN.QHI	0.03	370	0.00242	0.029 (1.99)	142 (9,746)
QRDQN.QHI	0.035	344	0.01121	0.031 (1.99)	153 (9,767)
TRPO.QHI	0.038	338	0.0154	0.038 (2.02)	185 (9,897)
A2C.QHI	0.042	344	0.01121	0.045 (2.02)	222 (9,902)
DQN.F	-0.417	40	0.99996	-0.401 (0.49)	-1,966 (2,408)
QRDQN.F	-0.42	48	0.99993	-0.42 (0.47)	-2,059 (2,322)
TRPO.F	-0.062	103	0.99625	-0.061 (1.9)	-297 (9,322)
A2C.F	-0.063	101	0.99669	-0.062 (1.9)	-302 (9,304)
DQN.QHI.F	-1.895	1	1	-1.901 (0)	-9,317 (0)
QRDQN.QHI.F	0.014	238	0.45904	0.012 (1.61)	61 (7,876)
TRPO.QHI.F	0.046	345	0.01062	0.048 (2.02)	236 (9,886)
A2C.QHI.F	0.036	343	0.01183	0.038 (2.02)	187 (9,915)
DET.TRPO.QHI	-0.662	57	0.99985	-0.579 (0)	-2,835 (2)
DET.A2C.QHI	-0.886	90	0.99837	-0.794 (0.16)	-3,888 (807)
DET.TRPO.QHI.F	0.032	271	0.21723	0.034 (1.83)	168 (8,948)
DET.A2C.QHI.F	0.02	287	0.13335	0.021 (2.01)	104 (9,836)

Table 3: Comparison between the average return of each counterfactual policy and that of the NWS policy on the evaluation years, summarized across counties (e.g. “Median Diff.” is the median difference in average return). The last two columns also provide a comparison to the counterfactual with zero heat alerts. WMW is the Wilcoxon-Mann-Whitney statistic (higher is better); its associated p-value is also included. The first policy, marked by *, requires oracle knowledge of the future weather. The approximate total number of hospitalizations is based on 49 million Medicare enrollees in 2011 (CMS, 2011).

tions are not perfect, but we start with perfect future information as a proof of concept. The names of models that include future information have the suffix “.F”.

5.3 Results and Discussion

Table 3 provides the main results of our RL experiments.

QHI restriction is necessary for the standard RL algorithms to perform well Several counterfactual policies perform worse than NWS (as indicated by negative median differences in returns): RANDOM, BASIC.NWS, and the RL models without the QHI restriction. By contrast, the RL models with the QHI restriction perform significantly better than NWS, as indicated by their significant positive median difference in returns. In absolute terms, a rough estimate if A2C.QHI were implemented as-is across all counties in the U.S. (using the Medicare population from 2011, the midpoint of our study period) is that we could see a reduction of 222 NOHR hospitalizations per year (approximate 95% CI = (-491,

1,131); details of this CI calculation are in Appendix E). Detailed discussion of this absolute benefit to public health is in Appendix F.

The futility of including future information One takeaway from our sensitivity analysis is that the addition of future information to the state space of the RL models had different effects depending on the algorithm. Across both plain and QHI-restricted models, TRPO was the only one that benefited. While A2C was minimally impacted, QRDQN and DQN were made noticeably worse. The latter may be due to the future information dramatically increasing the size of the state space/neural network parameters, which our hyperparameter tuning did not fully counteract. This resulted in high variance, for example, even though DQN.QHI.F performed well in the tuning stage, it proceeded to issue zero alerts in all but one county in the final evaluation stage. For the TRPO models, the benefit observed with the use of future information would likely be smaller in practice due to forecast / prediction error—the simulation of which is beyond the scope of this paper. We also note that the behavior (as described in Section 5.4) of TRPO.QHI and TRPO.QHI.F is quite similar. Therefore, we focus on the RL models without future information in the rest of this paper.

The need for stochastic policies A second takeaway from our sensitivity analysis is that interpreting policies from the TRPO and A2C models deterministically fails in the heat alerts setting under our rewards model. This is because many of the policy functions’ estimated probabilities for issuing an alert are below 0.5, so always taking the action with the larger probability dramatically reduces the number of alerts issued—in some counties to zero. Note that policies which do not use all the alerts in their budget are penalized by the specification of our rewards model, resulting in DET.TRPO.QHI and DET.A2C.QHI no longer outperforming NWS with statistical significance across the 30 counties. (Inclusion of future information mitigates this issue, but the results are not nearly as good as their stochastic counterparts.) This finding raises the question: *Are stochastic policies palatable from a domain perspective?* On the one hand, it is less immediately satisfying that some aspect of heat alerts issuance would be left to chance. On the other hand, in the context of human-in-the-loop decision making—which would likely be the case for public organizations such as NWS (Stuart et al., 2022)—an algorithm reporting probabilities is more informative than reporting only a binary action. And in any case, if in the future a heat alerts RL model was running continuously online, it would likely need to utilize exploration (incorporating some randomness into its actions) to update itself over time.

Figure 4 illustrates how the different policies look in practice, specifically for a setting where utilizing RL is beneficial. Additional examples with a small alert budget and where utilizing RL is not beneficial are shown in figures S4 and S5 respectively.

Comparing policies that perform significantly better than NWS We note that the performance and behavior of DQN.QHI is practically identical to AA.QHI—not just in its numerical summary, but also in the policies it issues. QRDQN.QHI performs a bit better than DQN.QHI, but not as well as the stochastic policies. Between those, A2C.QHI performs better than TRPO.QHI, though their policies tend to display similar characteristics. Therefore, we focus on A2C.QHI as the best RL policy in the post-hoc analysis. The non-RL counterfactual policies that perform well are that of always issuing an alert on days above an optimized QHI threshold (AA.QHI) and of issuing alerts on the b hottest days of the summer (TOPK). We note that the ordering of the Wilcoxon-Mann-Whitney statistics for TOPK, AA.QHI, and

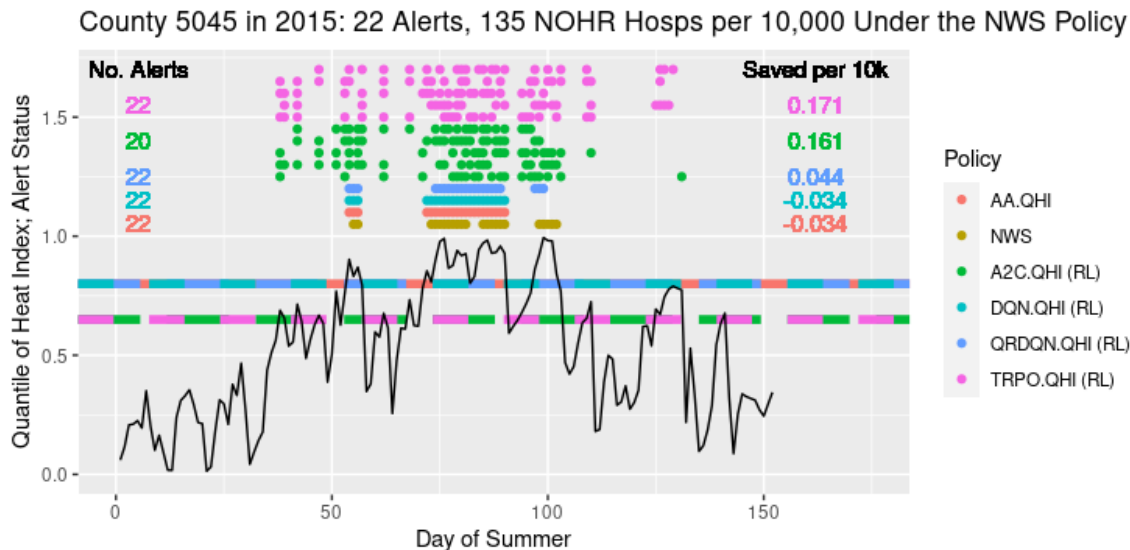


Figure 4: An example of observed and counterfactual heat alert policies for a single summer (2015 is the most recent year in our evaluation set), with estimates of the number of NOHR hospitalizations saved (compared to NWS) per 10,000 Medicare enrollees under each policy. The dashed lines indicate the optimized QHI threshold of the policy in the same color. The multiple horizontal lines of pink and green dots indicate five different samples from TRPO.QHI and A2C.QHI respectively. For these two policies, the number of NOHR hospitalizations saved is the average of all their evaluations over 2015.

A2C.QHI is opposite the ordering of these policies’ median difference in returns (compared to NWS). This is due to the longer tails of the A2C.QHI differences, as illustrated in Figure 6. For the interpretation of these results, recall that TOPK is an oracle policy. However, AA.QHI is an implementable alternative to A2C.QHI, so we must consider it more seriously.

5.4 Post-hoc Contrastive Explanation

To characterize differences between the best RL policies, the NWS policy, and alternative baselines, we consider both stationary features included upstream in the analysis (e.g., climate region and median household income) as well as characteristics of both the NWS and counterfactual alert policies, namely the distributions of the days of summer on which alerts are issued and the lengths of alert streaks (sequences of repeated alerts). We start with these alert characteristics, in Figure 5. In the histogram on the left, we see that both A2C.QHI and AA.QHI tend to issue heat alerts earlier in the summer than NWS. The histogram on the right indicates that A2C.QHI tends to issue shorter streaks of alerts (i.e., fewer consecutive days of alerts), which makes sense given its ability to learn sequential dependence encoded by the rewards model.

Figure 6 illustrates the varying performance of TOPK, AA.QHI, and A2C.QHI relative to the NWS policy across climate regions and counties. Note that large heterogeneity in the health effects of heat alert intervention across counties is consistent with previous findings (Wu et al., 2023). A striking visual pattern is the increasing vertical spread from left to

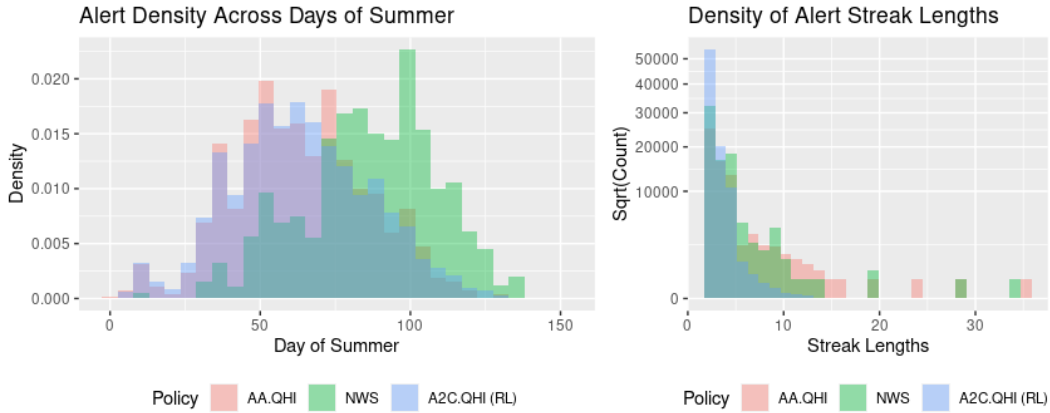


Figure 5: Distributions of heat alert characteristics under different policies, over the evaluation years.

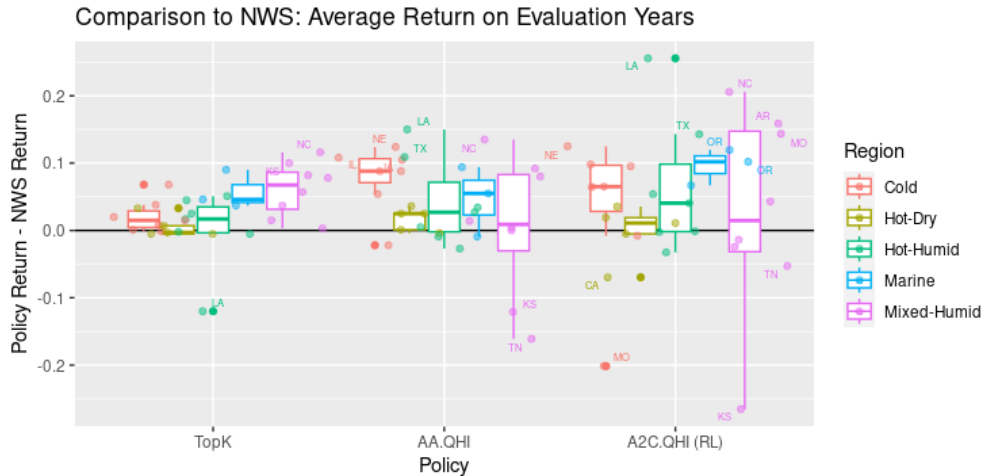


Figure 6: Different policies’ average return relative to NWS across different climate regions, over the evaluation years. Outlier points are labeled with their state abbreviation. Note that TOPK is an oracle policy.

right: TOPK performs the least heterogeneously across counties, followed by AA.QHI, and finally A2C.QHI. Similarly, some climate regions, such as Mixed-Humid and Hot-Humid, display more heterogeneity across counties than the others, across all the policies. This is partially due to those regions being larger and thus overrepresented among our 30 counties (see Table S2), but that does not fully explain the discrepancy.

To structure our investigation of why some counties see smaller (or even no) benefits from the application of the heat alerts RL, we fit CART on both the numeric difference in average return (compared to NWS) and a polytomous indicator of which policy performed the best. To prevent CART overfitting to our 30 counties and to facilitate interpretation, we ensure that the minimum number of counties in each leaf (terminal) node is greater than or equal to five for the regression and three for the polytomous classification.

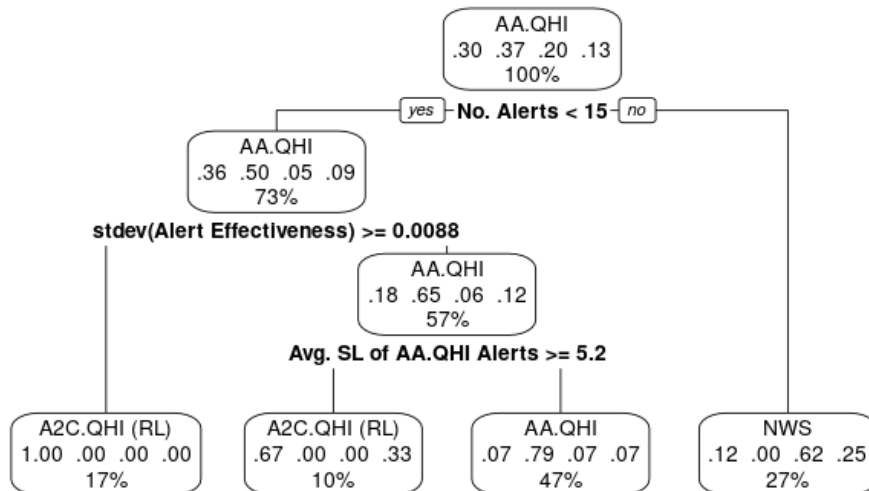


Figure 7: Polytomous classification tree comparing A2C.QHI, AA.QHI, NWS, and TRPO.QHI across the 30 counties. Within each node, the policy at the top is that associated with the highest probability of performing best. The four probabilities beneath correspond to the four policies in alphabetical order (as written above). The percentage at the bottom is the fraction of counties represented by that node. “No. Alerts” is the average number of heat alerts per warm season during the evaluation years, “Alert Effectiveness” is the τ estimated by our rewards model, and SL is the streak length.

RL performs best in counties with larger heat alert-health signal and longer heat waves A classification tree distinguishing A2C.QHI, AA.QHI, NWS, and TRPO.QHI is shown in Figure 7. Note that the two RL policies tend to be more similar to one another, as do the AA.QHI and NWS policies, so the distribution of probabilities is important to consider in addition to the overall classification of each node. Overall, the most predictive feature of the counterfactual policies’ performance relative to NWS is the size of the alert budget. The fact that the other policies find it harder to improve on NWS with more alerts may be because in such settings it is less critical to discriminate days when heat alerts will be most effective, given that our rewards model assumes more alerts never hurt in an absolute sense. The second split in the tree indicates that the RL performs best when there is greater variation in alert effectiveness across days, in other words, when there is more signal in the heat alert-health relationship that can be leveraged by the RL. This is an expected result. The third split highlights how it is better to use RL in counties that tend to experience more prolonged heat waves, which cause AA.QHI to issue more alerts in a row, increasing the likelihood of alert fatigue.

To provide more intuition for these insights, we ran the same polytomous classification on a set of more conventional covariates. The resulting Figure S6 shows a nearly-identical tree except with “Median Household Income \geq \$62,300” as the second split and “Region = Marine, Mixed-Humid” as the third split. The former suggests that median household income is an important contributor to alert effectiveness, which makes sense as people in lower-income areas may have less agency to take protective action in response to heat alerts,

such as turning on air conditioning. The latter suggests that humidity contributes to more prolonged heat waves, which makes sense given water’s high heat capacity slowing down the rate of temperature changes.

Additionally, RL performs better than NWS earlier in the summer Conducting regression on the difference in average returns between A2C.QHI and NWS using CART generated complementary insights. In Figure S7, the most predictive feature is the median day of summer on which the RL issued heat alerts. Specifically, A2C.QHI performs better in counties for which the RL identified that it is optimal to issue alerts earlier in the summer. Whereas, in counties for which it is optimal to issue alerts later in the summer, there was less room for improvement by the RL because the NWS already tends to issue alerts later in the summer. Among counties where the RL issued alerts earlier in the summer, A2C.QHI makes even more improvement over NWS in counties with higher alert budgets. Among counties where the RL issued alerts later in the summer, A2C.QHI still performs better than NWS in counties where NWS issues alerts in longer streaks—with similar intuition to the AA.QHI streaks.

6 Conclusion and Directions for Future Work

Contributions of this work to the field of RL were noted in Section 1. Here, we focus on our contributions laying the foundation of SDM for climate & health, namely (1) formulating and building an SDM pipeline to optimize heat alert issuance, which involved integrating traditional statistical methods with cutting-edge RL techniques and (2) offering insights into scenarios where RL improves vs. fails to improve on the NWS policy or simpler alternatives. We also identify directions for future research, motivated by our experiments.

Our first major conclusion from this analysis is that standard RL methods are inadequate to optimize the issuance of heat alerts for health. Even after simplifying the problem by considering only one county at a time, it was necessary to restrict alerts to days with higher QHI for the four RL algorithms (DQN, QRDQN, TRPO and A2C) to be effective. Our second major conclusion is that, with modifications to the RL workflow, we were able to identify alternative heat alert issuance strategies that outperform the NWS with statistical significance. Our post hoc contrastive analysis enabled an explanation of the RL’s performance heterogeneity, with reference to both the NWS policy and the simpler alternative AA.QHI. Future work might investigate the application of methods which ensure a new policy is never worse than the existing policy, such as safe policy learning or model predictive control. Alternatively, we could develop a predictive model to select counties that are likely to benefit from RL, using intuitions similar to those in our CART analysis.

In light of laying a foundation for sequential decision making in climate & health, we anticipate several common questions about our approach. The first is how to move beyond our fixed alert/intervention budget. Under climate change, the number of extreme heat events is likely to increase. How best to update an alert budget to address a changing system, while simultaneously managing alert fatigue, appears to be an open question. Future work could explore modeling alert fatigue as part of the RL environment, for instance, incorporating evidence and/or methods from behavioral science. Similarly, RL algorithms that are intentionally robust to distribution shift (i.e. under climate change) merit investigation in a climate & health setting.

A second question is whether *offline* (batch) RL methods, which use only observed data in place of a simulator, could be used to circumvent dependence on the specification of a rewards model. Several major challenges stand in the way of an offline approach, which we can highlight using the heat alerts case. First, there is a tension between trying to improve the observed policy and controlling distribution shift (Levine et al., 2020). In our heat alerts application, for instance, we see that NWS often issues alerts in streaks, making it hard for offline RL to learn and optimize the impact of an individual alert. Second, assessing the performance of offline RL models using off-policy evaluation (OPE) methods can be difficult. Aspects of the heat alerts setting which have been shown to challenge OPE methods include its long episodes, large potential for distribution shift (especially in the absence of a modification such as restricting alerts to very hot days), and high degree of autocorrelation in the reward (Uehara et al., 2022).

A third question is whether it is possible to formally quantify uncertainty around the number of hospitalizations that could be saved by implementing an RL policy. The answer to this has two dimensions. First, note that our method estimates how many lives could have been saved under past summers’ weather, not how many lives could be saved in future, which would necessitate projections of weather accounting for climate change. Second, while the Bayesian nature of our rewards model facilitates uncertainty quantification (as demonstrated by our calculation of an approximate confidence interval for the number of hospitalizations saved), estimating the additional uncertainty from sampling weather trajectories would require a procedure such as bootstrap. However, since we already used the regionally augmented weather trajectory data set for validation/tuning of our models, we are left with fairly limited data in the held-out final evaluation set.

A broader view of climate & health decision making is also valuable to consider. Ideally, an optimal heat alert system would account for different types of health impacts experienced by different demographic groups. Hence, future work could explore application of multi-objective RL to consider multiple kinds of health data or even proxies such as missed days of school and mobility data from smartphones / watches. Similarly, it is important to recognize that the issuance of heat alerts is only a first step towards reducing the public health impacts of extreme heat: there is much more work to be done analyzing and expanding local actions in response to heat alerts (Errett et al., 2023). If such on-the-ground interventions are able to increase the effectiveness of heat alerts, then this is likely to increase the ability of SDM methods such as RL to identify these effects and help us continue improving our strategies in the future.

Acknowledgments and Disclosure of Funding

This work was supported by an NSF Graduate Research Fellowship (EMC), NIH award K01ES032458 (RCN), NIH award R01-ES029950 (MT, GAW), NIH award 1R01MD016054-01A1 (FD), NIH award 5R01ES030616-04 (MT), NIH award 3RF1AG074372-01A1S1 (MT), NIH award P30ES000002 (MT), Alfred P. Sloan Foundation grant G-2020-13946 (FD), the Fernholz Foundation (MT), and Wellcome Trust grant 216033-Z-19-Z (GAW). We thank the National Studies on Air Pollution and Health research group for their support of this project. The computations in this paper were performed on the FASSE and FASRC Cannon

clusters supported by the FAS Division of Science Research Computing Group at Harvard University. Lastly, we acknowledge Kate Weinberger for facilitating access to the heat alerts data set, and the STAT 234 teaching staff at Harvard University for their feedback during early stages of this project. *Disclosures:* GAW currently serves as a consultant for the Health Effects Institute (Boston, MA) and recently served as a consultant for Google, LLC (Mountain View, CA).

Appendix A. Details of the Data Set

Evidence from the climate & health and environmental epidemiology literature guides our selection of relevant variables as well as feature engineering (described in Section 4.2).

A.1 Heat Alerts

Weinberger et al. (2021) and Wu et al. (2023) combined NWS heat “warnings” and “advisories” into the single category of “alerts”. In some locations, where the forecast zones in which the NWS issues alerts are smaller than county boundaries, the alert history was taken from whichever forecast zone contained the largest proportion of the 2010 county population.

A.2 Medicare Hospitalizations

The hospitalization claims data we use in this study is from Medicare Part A, fee-for-service. This data set covers the population aged 65 and older, who are enrolled in Medicare Part A, fee-for-service.⁴

A.3 Descriptive Statistics of Heat, Alerts, and Hospitalizations

Table S1 provides descriptive statistics of the heat alerts dataset, both for the 30 counties in our RL analysis and all the counties with population $\geq 65,000$ (used to create the BROACH environment). The two sets of statistics are similar aside from the number of heat alerts issued because the counties in the RL analysis were selected specifically for having issued higher numbers of alerts. Other observations are the long tail of the number of NWS alerts per county-summer, that some heat alerts were issued on days that were not very hot in an absolute or relative (quantile) sense, that there were some county-summers with few “hot” days (90th percentile by county⁵) and others with many, and that the distribution of day-of-summer for NWS heat alerts and 90th percentile QHI by county are quite similar. A few other relevant statistics not shown in the table are that (across all the counties) there were a total of 40,387 heat alerts issued between 2006 and 2016, that 17.2% of NWS heat alerts were issued on days with heat index values that were *not* in their county’s top 90th percentile, and that 74.0% of days in the top 90th QHI by county did not have NWS heat alerts.

⁴A 2021 report found that fee-for-service enrollees do not significantly differ from managed care enrollees (the rest of the Medicare population) (The Commonwealth Fund).

⁵Here, the 90th percentile was chosen to provide some intuition for the distribution of heat index and heat alerts. For context, Hondula et al. (2022) found that 95th percentile daily maximum heat index was the climatological indicator most strongly correlated with NWS heat alert frequency.

Variable	Min.	Q1	Median	Mean	Q3	Max.
*NOHR hosps per 1,000	5.4 (3.1)	12.5 (12.7)	14.8 (15.2)	15 (15.3)	17.3 (17.8)	25.7 (34.5)
*No. of NWS alerts	0 (0)	4 (0)	8 (3)	9.6 (4.8)	13 (7)	43 (57)
DMHI on alert days (°F)	70.5 (68.3)	100.3 (99.7)	103.5 (103.2)	102.5 (102.6)	106.2 (105.9)	121.1 (144)
Q-DMHI on alert days	18.9 (15.6)	91.6 (92.6)	95.8 (96.9)	93.4 (94.2)	98.2 (98.9)	100 (100)
*No. of 90th pct. HI days	0 (0)	9 (8)	14 (14)	15.4 (15.4)	21 (21)	46 (61)
DOS of NWS alerts	16 (2)	68 (69)	84 (84)	83.4 (83.5)	99 (99)	142 (150)
DOS of 90th pct. HI days	15 (1)	72 (69)	88 (85)	86.9 (85.2)	102 (102)	145 (153)

Table S1: Summary statistics for our 30 counties of interest (and all the counties) of Medicare NOHR hospitalizations, NWS heat alerts, heat index, and day of summer for several features of interest. DMHI = daily maximum heat index, Q-DMHI = county quantile of DMHI (referred to simply as QHI in the main text), DOS = day of summer (out of 152). Variables given per county-summer are marked with *.

Appendix B. Additional Details of the Bayesian Rewards Model

We now provide fine-grained details about the rewards model specification. In the vector of temporal covariates s_t , the piecewise linear expansion on QHI in λ (the baseline function) has knots at the 25th and 75th percentiles. In τ (the alert effectiveness function), we include only a linear term for QHI—again, conditional on day of summer and excess QHI (compared to the average of the last 3 days)—to both stabilize effect identification and facilitate interpretation. The spline on day of summer (with 3 degrees of freedom) is included in both λ and τ . Lastly, for the data-driven prior, we train one neural network for β (the coefficients of the baseline function) and another for δ (the coefficients of the alert effectiveness function). Both networks have one hidden layer with 32 units—this modest architecture avoids overfitting the relatively small number of spatial features in our dataset.

Results The rewards model clearly converged in its loss across epochs (shown in Figure S1) and achieved higher predictive accuracy than standard machine learning algorithms (i.e., random forest and neural network). Predicting the rate of NOHR hospitalizations in the Medicare population in each county, this model has $R^2 = 0.102$ —using the calculation SSR/SST for comparability with earlier machine learning models (such as that we used when checking the signal in the mortality data). Predicting the absolute number of NOHR hospitalizations, it has $R^2 = 0.884$ —much higher because the value is mostly driven by county population size. The model also displayed very good coverage when we ran it on synthetic data (1,000 samples from the posterior predictive) using known coefficients: average coverage across parameters for a 90% CI was 0.897.

Figure S2 shows one posterior sample across the 761 counties on which the model was fit. Note that the spread across counties is larger than the spread within counties, so the IQR bars are no larger for multiple samples. Overall, we see that the coefficients on past

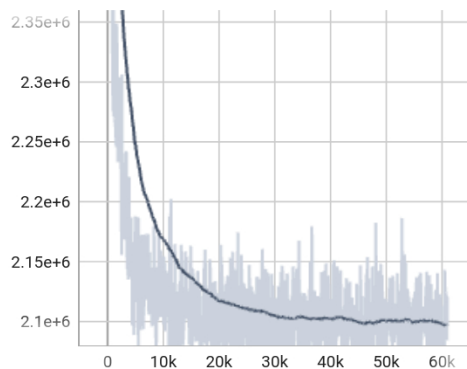


Figure S1: Convergence of the ELBO in the Bayesian rewards model during training (80 epochs).

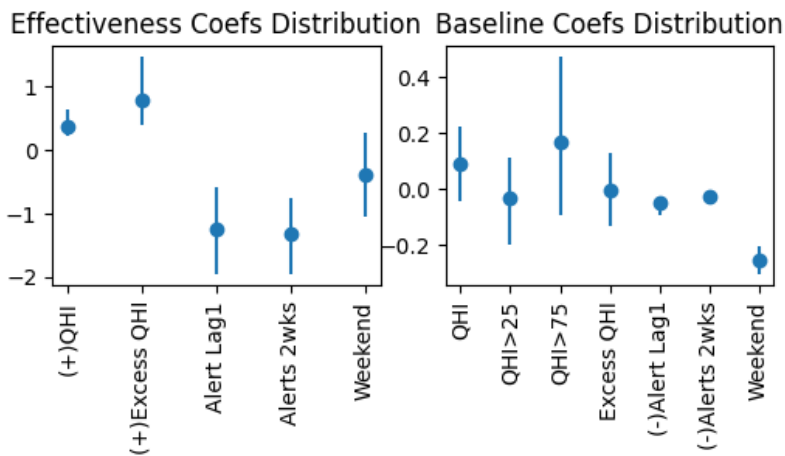


Figure S2: A sample of posterior coefficients from the rewards model (in τ and λ respectively), displaying IQR and median. Bias and coefficients for the spline on day of summer are not shown, for ease of interpretability. (+)/(-) indicates a coefficient constrained to be positive/negative.

alerts in today’s alert effectiveness (τ) are both negative, empirical evidence of alert fatigue. In the baseline hospitalization rate (λ), we see a strong protective effect by weekend.

Appendix C. Details of the RL Analysis

C.1 Selection of 30 Counties

Out of the 170 counties with 75 or more heat alerts issued between 2066 and 2016, we selected 30 using the following criteria: for each climate region⁶, select the county with the highest variance in estimated heat alert effectiveness. To get up to 30, repeat this selection,

⁶Excluding “Mixed Dry” and “Very Cold” because there were very few counties in these regions with sufficient population size

but first prioritize selecting a county from a U.S. state not already in the set, and if we must repeat a state, do not select a county that is directly adjacent to one already in the set. If there are no more eligible counties in a region, select from a larger region.

C.2 Hyperparameter Tuning

RL algorithms are known to be sensitive to their hyperparameters, especially in empirical settings (Eimer et al., 2022). To address this concern, we tuned hyperparameters per county, using the average return metric. First, we did a broad sweep on one county from each of the five climate regions using TRPO.QHI, experimenting with values of learning rate $\in \{0.01, 0.001, 0.0001\}$, discount factor $\in \{1.0, 0.999, 0.99\}$, neural network architecture (number of hidden layers $\in \{1, 2, 3\}$ and number of hidden units $\in \{16, 32, 64\}$), and size of the replay buffer $\in \{1024, 2048, 4096\}$; paired with possible QHI thresholds $\in \{0.55, 0.7, 0.85\}$ and both including and not including future information. After determining that learning rate=0.001 and discount factor=1.0 performed the best across the board, we tuned the remaining parameters for each county and each RL model (all combinations of TRPO, A2C, QRDQN and DQN with and without QHI restrictions and future information). To make the computation time more reasonable, we did a grid search on two values each for the number of hidden layers (2 or 3), number of hidden units (16 or 32), and size of the replay buffer (1,500 or 3,000). For QRDQN specifically, we also tested different values for the number of quantiles, which is closely tied to computation time for this algorithm. Using 10 quantiles rather than 20 ended up being not only faster but also better, potentially due to the latter overfitting.

Appendix D. Summary of the Workflow Using BROACH

This section is meant to illustrate a toy example of our workflow. Imagine seven counties located in two climate regions, as shown in the figure below. Let the training years $TY = \{2006, 2008, 2009, 2010, 2012, 2013, 2014, 2016\}$ and evaluation years $EY = \{2007, 2011, 2015\}$.

Climate Region A				Climate Region B		
1	2	3	4	5	6	7

First, train the rewards model on counties 1-7 and years $TY \cup EY$ to obtain posterior distributions for $r_1(s, a), \dots, r_7(s, a)$. Then, for each county, follow the steps below. Consider county 1 for illustration.

- 1: **if** Training RL (with a QHI restriction) **then**
- 2: **for** h in $\{0.5, 0.55, \dots, 0.9\}$ **do**
- 3: **for** i in 1 to N_T episodes **do**
- 4: Sample $r_{1,i}(s, a)$ from the posterior for $r_1(s, a)$
- 5: Sample $\xi_i \sim TY \times \{\xi_1, \xi_2, \xi_3, \xi_4\}$
- 6: Update $\pi_{1,h}(a|s)$ s.t. $a = 0$ if $QHI < h$, using $r_{1,i}$ and ξ_i

```

7:     end for
8:     Select  $\pi_{1,h}^*$  (across i) with the largest average return using  $\xi_i \sim EY \times \{\xi_2, \xi_3, \xi_4\}$ 
9:     end for
10: else if Tuning RL or AA.QHI then
11:   for h in {0.5, 0.55, ..., 0.9} do
12:     for i in 1 to  $N_E$  episodes do
13:       Sample  $r_{1,i}(s, a)$  from the posterior for  $r_1(s, a)$ 
14:       Sample  $\xi_i \sim EY \times \{\xi_2, \xi_3, \xi_4\}$ 
15:       Calculate cumulative reward using  $\pi_{1,h}^*$  (or AA.QHI with h),  $r_{1,i}$  and  $\xi_i$ 
16:     end for
17:   end for
18:   Select  $h^*$  with the largest return
19: else if Final evaluation for any policy (but using notation for optimized RL) then
20:   for i in 1 to  $N_E$  episodes do
21:     Sample  $r_{1,i}(s, a)$  from the posterior for  $r_1(s, a)$ 
22:     Sample  $\xi_i \sim EY \times \{\xi_1\}$ 
23:     Calculate cumulative reward using  $\pi_{1,h^*}^*$ ,  $r_{1,i}$  and  $\xi_i$ 
24:   end for
25: end if

```

Appendix E. Approximate Confidence Interval Calculation

To generate an approximate confidence interval for the absolute number of NOHR hospitalizations saved by implementing our best RL model, we use the estimates from the final evaluation for A2C.QHI and NWS. However, rather than first calculating average returns per county (across the 1,000 evaluation episodes) and then taking the median across the 30 counties, we first take the median return (across the 30 counties) from each of the 1,000 evaluation episodes and then calculate the 2.5% and 97.5% quantiles of the resulting distribution of medians.

Appendix F. Discussion of Absolute Public Health Benefits

Do we estimate substantive health benefits from implementing the improved heat alerts policies detailed in the main text?

For general context, the median rate of NOHR hospitalizations per 10,000 Medicare enrollees per summer during our study period was 148 (Table S1), and we estimated that deploying our best RL model *relative to issuing no heat alerts* would save 2 of these 148, or 1.4%, in the 30 counties in our RL analysis. Noting that the overall relative risk of a Medicare enrollee experiencing one of the NOHR hospitalization types on a heat wave day is about 1.10 (Bobb et al., 2014), this is substantial evidence in support of continuing to issue heat alerts to protect public health.

Compared to the observed NWS policy, A2C.QHI applied to the 30 counties in our analysis would save approximately 0.042 NOHR hospitalizations per 10,000 Medicare enrollees per summer, a reduction of only 0.03%. Multiplying this by 49 million, the size of the Medicare population in 2011 (the midpoint of our study period), yields about 222 NOHR hospital-

izations saved per summer. However, this modest value should be further contextualized by several points.

Firstly, heat alerts by themselves (and in our case, the re-arrangement of the same number of heat alerts) are a very cost-effective intervention, so even small reductions in health harms are promising.

Secondly, if we take into account the large heterogeneity in the benefit of RL across counties with numbers from the CART regression (Figure S7), assuming that we figure out how to implement a safe policy such that counties which would not benefit are unaffected, this number increases to 262 $((49\text{m}/10\text{k}) * (0.074 * 0.17 + 0.053 * 0.33 + 0.18 * 0.13))$ NOHR hospitalizations saved per summer. This is a rough approximation given that it assumes the proportion of counties in which RL alert policies were found to improve health outcomes in our sample is generalizable to the rest of the US. It is plausible that our sample of 30 counties is unrepresentative of the U.S. as they tend to have higher variability in alert effectiveness (increasing potential improvements from RL) and also higher alert budgets.

Thirdly, these metrics reflect the climate and Medicare population between 2006 and 2016. We confidently anticipate that both the frequency of extreme heat events under climate change and the size of the Medicare population will continue increasing (Dahl et al., 2019). For instance, while there were 49 million Medicare enrollees in 2011, by 2023 this number has increased to over 65 million, and by 2050 it is projected to be over 85 million (The Boards of Trustees of the Federal Hospital Insurance and Federal Supplementary Medical Insurance Trust Funds, 2023).

Fourthly, the numbers reported in this study should not be interpreted as the overall benefit to public health from improving heat alerts issuance strategies. The health data used in our study only reflect inpatient hospitalizations from NOHR causes billed to Medicare Part A, or hospital fee-for-service. Only about 60% of Medicare enrollees are in the fee-for-service population⁷, so hospitalizations of the other 40% do not appear in our dataset.

Appendix G. Supplemental Figures and Tables

⁷https://www.cms.gov/Research-Statistics-Data-and-Systems/Statistics-Trends-and-Reports/Beneficiary-Snapshot/Downloads/Bene_Snapnot.pdf

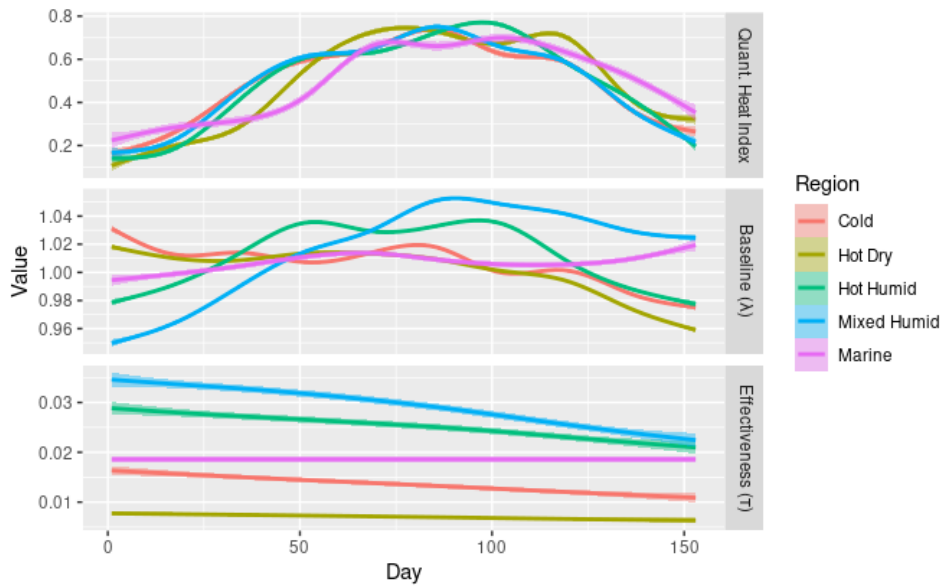


Figure S3: Smoothed trajectories of observed quantile of heat index, modeled baseline NOHR hospitalization rate, and modeled alert effectiveness (assuming no past alerts) across days of summer; colored by climate region. Note that λ and τ are normalized as they are in the RL reward function.

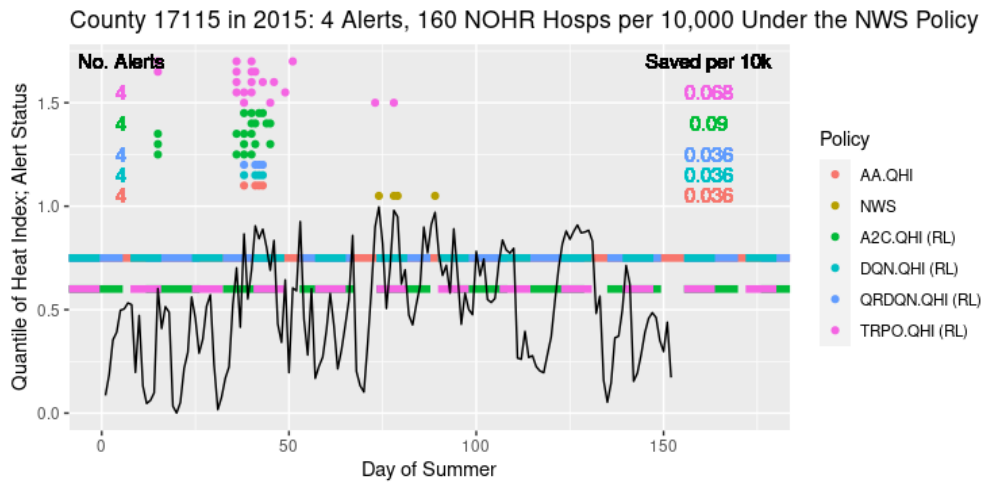


Figure S4: Example of a setting with relatively few heat alerts.

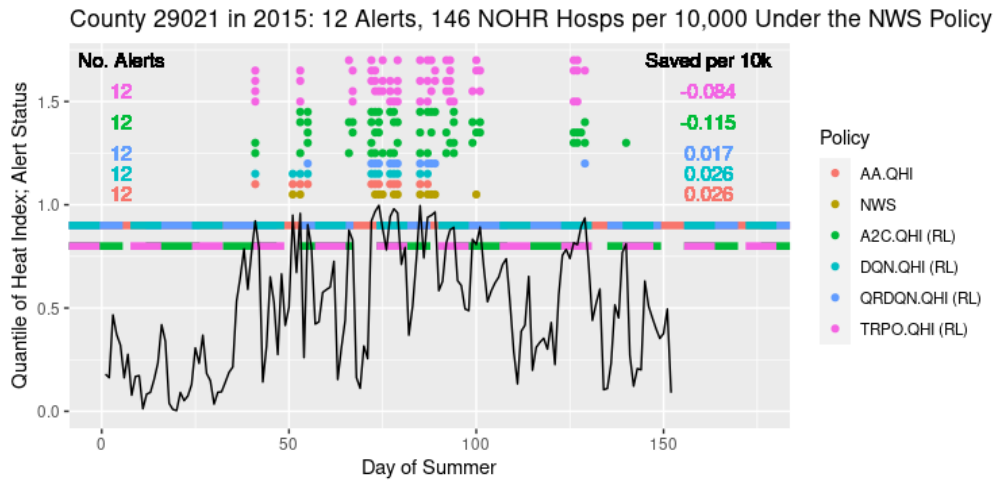


Figure S5: Example of a setting where implementing RL would not be beneficial relative to NWS or AA.QHI.

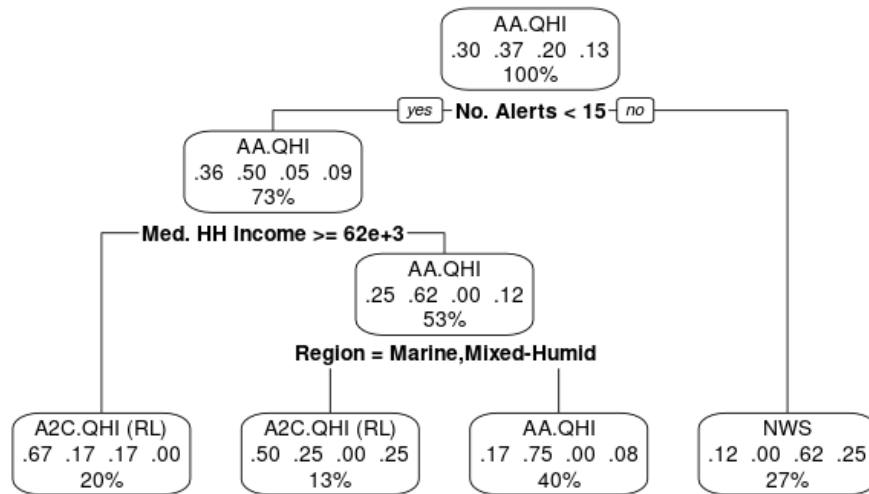


Figure S6: Polytomous classification tree comparing A2C.QHI, AA.QHI, NWS, and TRPO.QHI across the 30 counties—using more conventional features than Figure 7. Within each node, the policy at the top is that associated with the highest probability of performing best. The four probabilities beneath correspond to the four policies in alphabetical order (as written above). The percentage at the bottom is the fraction of counties represented by that node. “No. Alerts” is the average number of heat alerts per warm season during the evaluation years.

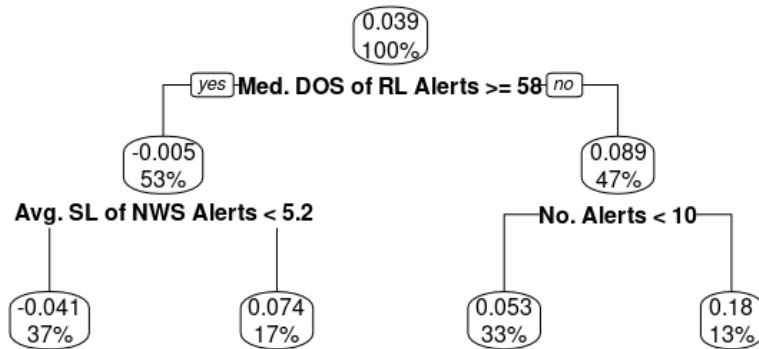


Figure S7: Regression tree on the differences in average return between A2C.QHI and NWS. Within each node, the number at the top is the prediction (average) difference, with positive indicating that the RL is better and negative indicating that the NWS is better. The percentage at the bottom is the fraction of counties represented by that node. DOS is the day of summer, SL is the streak length, and “No. Alerts” is the average number of heat alerts per warm season during the evaluation years.

County Fips (State name abbreviation)	Region	No. Alerts (Eval Years)	Population Density (/mi ²)	Median HH Income (USD)	Democratic Voters (%)	Broadband Usage (%)	Average PM _{2.5} ($\mu\text{g}/\text{m}^3$)
5045 (AR)	MxHd	61	179.00	50314.00	34.00	37.50	9.08
20161 (KS)	MxHd	47	120.00	43962.00	43.50	52.20	6.35
21059 (KY)	MxHd	24	212.00	46555.00	38.70	53.30	10.22
29019 (MO)	MxHd	50	242.00	48627.00	51.60	46.60	7.85
37085 (NC)	MxHd	31	200.00	44625.00	39.30	46.70	9.65
40017 (OK)	MxHd	63	133.00	63629.00	22.80	70.10	7.53
47113 (TN)	MxHd	58	176.00	41617.00	44.30	79.40	9.29
42017 (PA)	MxHd	25	1036.00	76555.00	51.00	85.10	9.14
41053 (OR)	Mrn	31	102.00	52808.00	45.60	79.20	3.24
41067 (OR)	Mrn	31	745.00	64180.00	57.70	82.70	4.28
53015 (WA)	Mrn	23	90.00	47596.00	49.40	53.60	3.59
13031 (GA)	HtHd	43	106.00	35840.00	38.90	57.50	9.01
22109 (LA)	HtHd	34	91.00	49960.00	27.90	55.50	8.26
28049 (MS)	HtHd	57	283.00	37626.00	69.90	36.50	8.50
45015 (SC)	HtHd	48	168.00	52427.00	41.20	66.20	8.72
48157 (TX)	HtHd	42	707.00	85297.00	47.80	83.70	8.64
48367 (TX)	HtHd	41	131.00	64515.00	18.30	52.20	7.84
22063 (LA)	HtHd	42	201.00	56811.00	13.70	47.60	8.87
4015 (AZ)	HtDr	29	15.00	39200.00	28.70	63.60	4.59
6025 (CA)	HtDr	40	42.00	41807.00	64.00	64.40	7.22
32003 (NV)	HtDr	29	251.00	52873.00	55.90	78.10	5.21
4013 (AZ)	HtDr	72	423.00	53596.00	44.00	77.40	6.38
6071 (CA)	HtDr	29	103.00	54090.00	51.60	77.10	6.38
17115 (IL)	Cold	22	190.00	46559.00	45.70	63.60	8.87
17167 (IL)	Cold	25	228.00	55449.00	46.00	66.50	8.75
19153 (IA)	Cold	24	764.00	59018.00	54.90	57.90	8.25
19155 (IA)	Cold	27	98.00	51304.00	44.30	42.00	7.89
34021 (NJ)	Cold	29	1639.00	73480.00	67.30	81.60	9.31
29021 (MO)	Cold	44	219.00	44363.00	43.70	48.80	7.97
31153 (NE)	Cold	27	681.00	69965.00	37.60	72.60	7.92

Table S2: Descriptive statistics of the 30 counties used in policy optimization. Climate region abbreviations = {MxHD: Mixed-Humid, Mrn: Marine, HtHd: Hot-Humid, HtDr: Hot-Dry, Cold: Cold}. HH = household. PM_{2.5} is an annual average.

References

- Anish Agarwal, Abdullah Alomar, Varkey Alumootil, Devavrat Shah, Dennis Shen, Zhi Xu, and Cindy Yang. PerSim: Data-Efficient Offline Reinforcement Learning with Heterogeneous Agents via Personalized Simulators. In *Advances in Neural Information Processing Systems*, volume 34, pages 18564–18576. Curran Associates, Inc., 2021. URL <https://proceedings.neurips.cc/paper/2021/hash/9a3f263a5e5f63006098a05cd7491997-Abstract.html>.
- G. Brooke Anderson and Michelle L. Bell. Heat Waves in the United States: Mortality Risk during Heat Waves and Effect Modification by Heat Wave Characteristics in 43 U.S. Communities. *Environmental Health Perspectives*, 119(2):210–218, February 2011. ISSN 0091-6765, 1552-9924. doi: 10.1289/ehp.1002313. URL <https://ehp.niehs.nih.gov/doi/10.1289/ehp.1002313>.
- Susan C. Anenberg, Shannon Haines, Elizabeth Wang, Nicholas Nassikas, and Patrick L. Kinney. Synergistic health effects of air pollution, temperature, and pollen exposure: a systematic review of epidemiological evidence. *Environmental Health*, 19:130, December 2020. ISSN 1476-069X. doi: 10.1186/s12940-020-00681-z. URL <https://www.ncbi.nlm.nih.gov/pmc/articles/PMC7720572/>.
- Peter C Austin. A tutorial on multilevel survival analysis: methods, models and applications. *International Statistical Review*, 85(2):185–203, 2017.
- Andrew Bell and Kelvyn Jones. Explaining fixed effects: Random effects modeling of time-series cross-sectional and panel data. *Political Science Research and Methods*, 3(1): 133–153, 2015.
- Dimitri Bertsekas and Steven E Shreve. *Stochastic optimal control: the discrete-time case*, volume 5. Athena Scientific, 1996.
- Jennifer F. Bobb, Ziad Obermeyer, Yun Wang, and Francesca Dominici. Cause-Specific Risk of Hospital Admission Related to Extreme Heat in Older Adults. *JAMA*, 312(24): 2659–2667, December 2014. ISSN 0098-7484. doi: 10.1001/jama.2014.15715. URL <https://doi.org/10.1001/jama.2014.15715>.
- A Colin Cameron and Pravin K Trivedi. *Regression analysis of count data*, volume 53. Cambridge university press, 2013.
- Nicolas Carrara, Edouard Leurent, Romain Laroche, Tanguy Urvoy, Odalric-Ambrym Mailhard, and Olivier Pietquin. Budgeted reinforcement learning in continuous state space. *Advances in Neural Information Processing Systems*, 32, 2019.
- CMS. 2011 cms statistics. Technical report, U.S. Department of Health and Human Services, 2011. URL https://www.cms.gov/Research-Statistics-Data-and-Systems/Statistics-Trends-and-Reports/CMS-Statistics-Reference-Booklet/Downloads/CMS_Stats_2011.pdf.

- Matthew J. Cutler, Jennifer R. Marlon, Peter D. Howe, and Anthony Leiserowitz. The Influence of Political Ideology and Socioeconomic Vulnerability on Perceived Health Risks of Heat Waves in the Context of Climate Change. *Weather, Climate, and Society*, 10(4): 731–746, October 2018. ISSN 1948-8327, 1948-8335. doi: 10.1175/WCAS-D-17-0105.1. URL <https://journals.ametsoc.org/doi/10.1175/WCAS-D-17-0105.1>.
- Kristina Dahl, Rachel Licker, John T Abatzoglou, and Juan Declet-Barreto. Increased frequency of and population exposure to extreme heat index days in the United States during the 21st century. *Environmental Research Communications*, 1(7):075002, August 2019. ISSN 2515-7620. doi: 10.1088/2515-7620/ab27cf. URL <https://iopscience.iop.org/article/10.1088/2515-7620/ab27cf>.
- Kristie L. Ebi, Thomas J. Teisberg, Laurence S. Kalkstein, Lawrence Robinson, and Rodney F. Weiher. Heat Watch/Warning Systems Save Lives: Estimated Costs and Benefits for Philadelphia 1995–98. *Bulletin of the American Meteorological Society*, 85(8):1067–1074, August 2004. ISSN 0003-0007, 1520-0477. doi: 10.1175/BAMS-85-8-1067. URL <https://journals.ametsoc.org/doi/10.1175/BAMS-85-8-1067>.
- Kristie L Ebi, Anthony Capon, Peter Berry, Carolyn Broderick, Richard de Dear, George Havenith, Yasushi Honda, R Sari Kovats, Wei Ma, Arunima Malik, Nathan B Morris, Lars Nybo, Sonia I Seneviratne, Jennifer Vanos, and Ollie Jay. Hot weather and heat extremes: health risks. *The Lancet*, 398(10301):698–708, August 2021. ISSN 01406736. doi: 10.1016/S0140-6736(21)01208-3. URL <https://linkinghub.elsevier.com/retrieve/pii/S0140673621012083>.
- Yonathan Efroni, Dylan J Foster, Dipendra Misra, Akshay Krishnamurthy, and John Langford. Sample-efficient reinforcement learning in the presence of exogenous information. In *Conference on Learning Theory*, pages 5062–5127, 2022.
- Theresa Eimer, Carolin Benjamins, and Marius Lindauer. Hyperparameters in Contextual RL are Highly Situational, December 2022. URL <http://arxiv.org/abs/2212.10876>. arXiv:2212.10876 [cs].
- Nicole A. Errett, Cat Hartwell, Juliette M. Randazza, Amruta Nori-Sarma, Kate R. Weinberger, Keith R. Spangler, Yuantong Sun, Quinn H. Adams, Gregory A. Wellenius, and Jeremy J. Hess. Survey of extreme heat public health preparedness plans and response activities in the most populous jurisdictions in the United States. *BMC public health*, 23(1):811, May 2023. ISSN 1471-2458. doi: 10.1186/s12889-023-15757-x.
- Jordan Frank, Shie Mannor, and Doina Precup. Reinforcement learning in the presence of rare events. In *Proceedings of the 25th international conference on Machine learning*, pages 336–343, 2008.
- Andrew Gelman. Prior distributions for variance parameters in hierarchical models (comment on article by browne and draper). *Bayesian Analysis*, 1(3):515–534, 2006.
- Soumyajit Guin and Shalabh Bhatnagar. A policy gradient approach for finite horizon constrained markov decision processes. In *2023 62nd IEEE Conference on Decision and Control (CDC)*, pages 3353–3359. IEEE, 2023.

- Melanie S. Hammer, Aaron van Donkelaar, Chi Li, Alexei Lyapustin, Andrew M. Sayer, N. Christina Hsu, Robert C. Levy, Michael J. Garay, Olga V. Kalashnikova, Ralph A. Kahn, Michael Brauer, Joshua S. Apte, Daven K. Henze, Li Zhang, Qiang Zhang, Bonne Ford, Jeffrey R. Pierce, and Randall V. Martin. Global Estimates and Long-Term Trends of Fine Particulate Matter Concentrations (1998–2018). *Environmental Science & Technology*, 54(13):7879–7890, July 2020. ISSN 0013-936X. doi: 10.1021/acs.est.0c01764. URL <https://doi.org/10.1021/acs.est.0c01764>. Publisher: American Chemical Society.
- Dong Han, Beni Mulyana, Vladimir Stankovic, and Samuel Cheng. A Survey on Deep Reinforcement Learning Algorithms for Robotic Manipulation. *Sensors (Basel, Switzerland)*, 23(7):3762, April 2023. ISSN 1424-8220. doi: 10.3390/s23073762. URL <https://www.ncbi.nlm.nih.gov/pmc/articles/PMC10098871/>.
- Alice Harpole, Michael Zingale, Ian Hawke, and Taher Chegini. pyro: a framework for hydrodynamics explorations and prototyping. *Journal of Open Source Software*, 4(34):1265, 2019. doi: 10.21105/joss.01265. URL <https://doi.org/10.21105/joss.01265>.
- Michelle D. Hawkins, Vankita Brown, and Jannie Ferrell. Assessment of NOAA National Weather Service Methods to Warn for Extreme Heat Events. *Weather, Climate, and Society*, 9(1):5–13, January 2017. ISSN 1948-8327, 1948-8335. doi: 10.1175/WCAS-D-15-0037.1. URL <https://journals.ametsoc.org/doi/10.1175/WCAS-D-15-0037.1>.
- Seulkee Heo, Michelle L. Bell, and Jong-Tae Lee. Comparison of health risks by heat wave definition: Applicability of wet-bulb globe temperature for heat wave criteria. *Environmental Research*, 168:158–170, January 2019. ISSN 00139351. doi: 10.1016/j.envres.2018.09.032. URL <https://linkinghub.elsevier.com/retrieve/pii/S0013935118305188>.
- Alexandre Heuillet, Fabien Couthouis, and Natalia Díaz-Rodríguez. Explainability in deep reinforcement learning. *Knowledge-Based Systems*, 214:106685, February 2021. ISSN 0950-7051. doi: 10.1016/j.knosys.2020.106685. URL <https://www.sciencedirect.com/science/article/pii/S0950705120308145>.
- David M. Hondula, Samuel Meltzer, Robert C. Balling, and Paul Iñiguez. Spatial Analysis of United States National Weather Service Excessive Heat Warnings and Heat Advisories. *Bulletin of the American Meteorological Society*, 103(9):E2017–E2031, September 2022. ISSN 0003-0007, 1520-0477. doi: 10.1175/BAMS-D-21-0069.1. URL <https://journals.ametsoc.org/view/journals/bams/103/9/BAMS-D-21-0069.1.xml>. Publisher: American Meteorological Society Section: Bulletin of the American Meteorological Society.
- Eric B. Laber, Fan Wu, Catherine Munera, Ilya Lipkovich, Salvatore Colucci, and Steve Ripa. Identifying optimal dosage regimes under safety constraints: An application to long term opioid treatment of chronic pain. *Statistics in Medicine*, 37(9):1407–1418, 2018. ISSN 1097-0258. doi: 10.1002/sim.7566. URL <https://onlinelibrary.wiley.com/doi/abs/10.1002/sim.7566>. eprint: <https://onlinelibrary.wiley.com/doi/pdf/10.1002/sim.7566>.

- Jonathan N. Lee, Alekh Agarwal, Christoph Dann, and Tong Zhang. Learning in POMDPs is Sample-Efficient with Hindsight Observability, February 2023. URL <http://arxiv.org/abs/2301.13857>. arXiv:2301.13857 [cs, stat].
- Sergey Levine, Aviral Kumar, George Tucker, and Justin Fu. Offline Reinforcement Learning: Tutorial, Review, and Perspectives on Open Problems. *arXiv:2005.01643 [cs, stat]*, November 2020. URL <http://arxiv.org/abs/2005.01643>. arXiv: 2005.01643.
- Yexin Li, Yu Zheng, and Qiang Yang. Dynamic Bike Reposition: A Spatio-Temporal Reinforcement Learning Approach. In *Proceedings of the 24th ACM SIGKDD International Conference on Knowledge Discovery & Data Mining*, pages 1724–1733, London United Kingdom, July 2018. ACM. ISBN 978-1-4503-5552-0. doi: 10.1145/3219819.3220110. URL <https://dl.acm.org/doi/10.1145/3219819.3220110>.
- Peng Liao, Kristjan Greenewald, Predrag Klasnja, and Susan Murphy. Personalized Heart-Steps: A Reinforcement Learning Algorithm for Optimizing Physical Activity. *Proceedings of the ACM on Interactive, Mobile, Wearable and Ubiquitous Technologies*, 4(1):18:1–18:22, March 2020. doi: 10.1145/3381007. URL <https://doi.org/10.1145/3381007>.
- Pierre Masselot, Fateh Chebana, Céline Campagna, Eric Lavigne, Taha B.M.J. Ouarda, and Pierre Gosselin. Machine Learning Approaches to Identify Thresholds in a Heat-Health Warning System Context. *Journal of the Royal Statistical Society Series A: Statistics in Society*, 184(4):1326–1346, October 2021. ISSN 0964-1998. doi: 10.1111/rssa.12745. URL <https://doi.org/10.1111/rssa.12745>.
- Kristina B. Metzger, Kazuhiko Ito, and Thomas D. Matte. Summer Heat and Mortality in New York City: How Hot Is Too Hot? *Environmental Health Perspectives*, 118(1): 80–86, January 2010. ISSN 0091-6765, 1552-9924. doi: 10.1289/ehp.0900906. URL <https://ehp.niehs.nih.gov/doi/10.1289/ehp.0900906>.
- Microsoft AI for Good Research Lab. U.S. Broadband Usage Percentages Dataset, 2021. URL <https://github.com/microsoft/USBroadbandUsagePercentages>.
- MIT Election Data and Science Lab. County Presidential Election Returns 2000-2020, 2018. URL <https://doi.org/10.7910/DVN/VOQCHQ>.
- Tong Mu, Georgios Theodorou, David Arbour, and Emma Brunskill. Constraint Sampling Reinforcement Learning: Incorporating Expertise For Faster Learning, December 2021. URL <http://arxiv.org/abs/2112.15221>. arXiv:2112.15221 [cs].
- Inbal Nahum-Shani, Shawna N Smith, Bonnie J Spring, Linda M Collins, Katie Witkiewitz, Ambuj Tewari, and Susan A Murphy. Just-in-Time Adaptive Interventions (JITAs) in Mobile Health: Key Components and Design Principles for Ongoing Health Behavior Support. *Annals of Behavioral Medicine: A Publication of the Society of Behavioral Medicine*, 52(6):446–462, December 2017. ISSN 0883-6612. doi: 10.1007/s12160-016-9830-8. URL <https://www.ncbi.nlm.nih.gov/pmc/articles/PMC5364076/>.
- Sanjana Narayanan, Isaac Lage, and Finale Doshi-Velez. (When) Are Contrastive Explanations of Reinforcement Learning Helpful?, November 2022. URL <http://arxiv.org/abs/2211.07719>. arXiv:2211.07719 [cs].

- Chris Fook Sheng Ng, Kayo Ueda, Ayano Takeuchi, Hiroshi Nitta, Shoko Konishi, Rinako Bagrowicz, Chiho Watanabe, and Akinori Takami. Sociogeographic Variation in the Effects of Heat and Cold on Daily Mortality in Japan. *Journal of Epidemiology*, 24(1): 15–24, 2014. ISSN 0917-5040, 1349-9092. doi: 10.2188/jea.JE20130051. URL https://www.jstage.jst.go.jp/article/jea/24/1/24_JE20130051/_article.
- Widemberg S Nobre, Alexandra M Schmidt, and João BM Pereira. On the effects of spatial confounding in hierarchical models. *International Statistical Review*, 89(2):302–322, 2021.
- Sindhu Padakandla. A survey of reinforcement learning algorithms for dynamically varying environments. *ACM Computing Surveys (CSUR)*, 54(6):1–25, 2021.
- Judea Pearl. The mediation formula: A guide to the assessment of causal pathways in nonlinear models. *Causality: Statistical perspectives and applications*, pages 151–179, 2012.
- Erika Puiutta and Eric MSP Veith. Explainable Reinforcement Learning: A Survey, May 2020. URL <http://arxiv.org/abs/2005.06247>. arXiv:2005.06247 [cs, stat].
- Martin L Puterman. *Markov decision processes: discrete stochastic dynamic programming*. John Wiley & Sons, 2014.
- Antonin Raffin, Ashley Hill, Adam Gleave, Anssi Kanervisto, Maximilian Ernestus, and Noah Dormann. Stable-baselines3: Reliable reinforcement learning implementations. *Journal of Machine Learning Research*, 22(268):1–8, 2021. URL <http://jmlr.org/papers/v22/20-1364.html>.
- Alex Ray, Joshua Achiam, and Dario Amodei. Benchmarking Safe Exploration in Deep Reinforcement Learning. 2019.
- Joshua Romoff, Peter Henderson, Alexandre Piche, Vincent Francois-Lavet, and Joelle Pineau. Reward estimation for variance reduction in deep reinforcement learning. In *Conference on Robot Learning*, pages 674–699. PMLR, 2018.
- Donald B Rubin. Causal inference using potential outcomes: Design, modeling, decisions. *Journal of the American Statistical Association*, 100(469):322–331, 2005.
- Sean R. Sinclair, Felipe Vieira Frujeri, Ching-An Cheng, Luke Marshall, Hugo De Oliveira Barbalho, Jingling Li, Jennifer Neville, Ishai Menache, and Adith Swaminathan. Hind-sight learning for MDPs with exogenous inputs. In Andreas Krause, Emma Brunskill, Kyunghyun Cho, Barbara Engelhardt, Sivan Sabato, and Jonathan Scarlett, editors, *Proceedings of the 40th International Conference on Machine Learning*, volume 202 of *Proceedings of Machine Learning Research*, pages 31877–31914. PMLR, 23–29 Jul 2023. URL <https://proceedings.mlr.press/v202/sinclair23a.html>.
- Neil A. Stuart, Gail Hartfield, David M. Schultz, Katie Wilson, Gregory West, Robert Hoffman, Gary Lackmann, Harold Brooks, Paul Roebber, Teresa Bals-Elsholz, Holly

- Obermeier, Falko Juddt, Patrick Market, Daniel Nietfeld, Bruce Telfeyan, Dan DePodwin, Jeffrey Fries, Elliot Abrams, and Jerry Shields. The Evolving Role of Humans in Weather Prediction and Communication. *Bulletin of the American Meteorological Society*, 103(8):E1720–E1746, August 2022. ISSN 0003-0007, 1520-0477. doi: 10.1175/BAMS-D-20-0326.1. URL <https://journals.ametsoc.org/view/journals/bams/103/8/BAMS-D-20-0326.1.xml>. Publisher: American Meteorological Society Section: Bulletin of the American Meteorological Society.
- Richard S. Sutton and Andrew G. Barto. *Reinforcement Learning: An Introduction*. The MIT Press, second edition, 2018. URL <http://incompleteideas.net/book/the-book-2nd.html>.
- Richard S Sutton, David McAllester, Satinder Singh, and Yishay Mansour. Policy gradient methods for reinforcement learning with function approximation. *Advances in neural information processing systems*, 12, 1999.
- Mauricio Tec, Yunshan Duan, and Peter Müller. A comparative tutorial of bayesian sequential design and reinforcement learning. *The American Statistician*, 77(2):223–233, 2023.
- Mauricio Tec, Ana Trisovic, Michelle Audirac, Sophie Woodward, Jie Kate Hu, Naeem Khoshnevis, and Francesca Dominici. Space: The spatial confounding environment. In *International Conference in Learning Representations (ICLR)*, 2024.
- The Boards of Trustees of the Federal Hospital Insurance and Federal Supplementary Medical Insurance Trust Funds. 2023 annual report. Technical report, Centers for Medicare & Medicaid Services, 2023. URL <https://www.cms.gov/oact/tr/2023>.
- The Commonwealth Fund. Medicare advantage vs. traditional medicare: How do beneficiaries’ characteristics and experiences differ? URL <https://www.commonwealthfund.org/publications/issue-briefs/2021/oct/medicare-advantage-vs-traditional-medicare-beneficiaries-differ>. Accessed: 2024-01-01.
- Marcin Tomczak, Siddharth Swaroop, and Richard Turner. Efficient Low Rank Gaussian Variational Inference for Neural Networks. In *Advances in Neural Information Processing Systems*, volume 33, pages 4610–4622. Curran Associates, Inc., 2020. URL <https://proceedings.neurips.cc/paper/2020/hash/310cc7ca5a76a446f85c1a0d641ba96d-Abstract.html>.
- Mark Towers, Jordan K. Terry, Ariel Kwiatkowski, John U. Balis, Gianluca de Cola, Tristan Deleu, Manuel Goulão, Andreas Kallinteris, Arjun KG, Markus Krimmel, Rodrigo Perez-Vicente, Andrea Pierré, Sander Schulhoff, Jun Jet Tai, Andrew Tan Jin Shen, and Omar G. Younis. Gymnasium, March 2023. URL <https://zenodo.org/record/8127025>.
- Dimitris G Tzikas, Aristidis C Likas, and Nikolaos P Galatsanos. The variational approximation for bayesian inference. *IEEE Signal Processing Magazine*, 25(6):131–146, 2008.

- Masatoshi Uehara, Chengchun Shi, and Nathan Kallus. A Review of Off-Policy Evaluation in Reinforcement Learning, December 2022. URL <http://arxiv.org/abs/2212.06355>. arXiv:2212.06355 [cs, math, stat].
- U.S. Census Bureau. 2009-2013 American Community Survey 5-year County-level Estimates of Population and Median Household Income, 2014.
- U.S. Energy Information Administration. Climate Zones - DOE Building America Program, 2020. URL <https://atlas.eia.gov/datasets/eia::climate-zones-doe-building-america-program/about>.
- Jasper van der Waa, Jurriaan van Diggelen, Karel van den Bosch, and Mark Neerincx. Contrastive Explanations for Reinforcement Learning in terms of Expected Consequences, July 2018. URL <http://arxiv.org/abs/1807.08706>. arXiv:1807.08706 [cs, stat].
- Yixin Wang, Andrew C. Miller, and David M. Blei. Comment: Variational autoencoders as empirical bayes. *Statistical Science*, 34(2):229–233, 2019. doi: 10.1214/19-sts710.
- Kate R. Weinberger, Antonella Zanobetti, Joel Schwartz, and Gregory A. Wellenius. Effectiveness of National Weather Service heat alerts in preventing mortality in 20 US cities. *Environment International*, 116:30–38, July 2018. ISSN 0160-4120. doi: 10.1016/j.envint.2018.03.028. URL <https://www.sciencedirect.com/science/article/pii/S0160412017320354>.
- Kate R. Weinberger, Xiao Wu, Shengzhi Sun, Keith R. Spangler, Amruta Nori-Sarma, Joel Schwartz, Weeberb Requia, Benjamin M. Sabbath, Danielle Braun, Antonella Zanobetti, Francesca Dominici, and Gregory A. Wellenius. Heat warnings, mortality, and hospital admissions among older adults in the United States. *Environment International*, 157: 106834, December 2021. ISSN 01604120. doi: 10.1016/j.envint.2021.106834. URL <https://linkinghub.elsevier.com/retrieve/pii/S0160412021004591>.
- Qiong Wu, Xu Chen, Zhi Zhou, Liang Chen, and Junshan Zhang. Deep Reinforcement Learning With Spatio-Temporal Traffic Forecasting for Data-Driven Base Station Sleep Control. *IEEE/ACM Transactions on Networking*, 29(2):935–948, April 2021. ISSN 1063-6692, 1558-2566. doi: 10.1109/TNET.2021.3053771. URL <https://ieeexplore.ieee.org/document/9340607/>.
- Xiao Wu, Kate R. Weinberger, Gregory A. Wellenius, Francesca Dominici, and Danielle Braun. Assessing the causal effects of a stochastic intervention in time series data: are heat alerts effective in preventing deaths and hospitalizations? *Biostatistics*, February 2023. URL <https://doi-org.ezp-prod1.hul.harvard.edu/10.1093/biostatistics/kxad002>.
- Haoran Xu, Xianyuan Zhan, and Xiangyu Zhu. Constraints Penalized Q-learning for Safe Offline Reinforcement Learning, April 2022. URL <http://arxiv.org/abs/2107.09003>. arXiv:2107.09003 [cs].
- Tristan Zajonc. Bayesian Inference for Dynamic Treatment Regimes: Mobility, Equity, and Efficiency in Student Tracking. *Journal of the American Statistical Association*, 107(497):

80–92, March 2012. ISSN 0162-1459, 1537-274X. doi: 10.1080/01621459.2011.643747.
URL <http://www.tandfonline.com/doi/abs/10.1080/01621459.2011.643747>.

Antonella Zanobetti, Marie S. O’Neill, Carina J. Gronlund, and Joel D Schwartz. Susceptibility to Mortality in Weather Extremes: Effect Modification by Personal and Small Area Characteristics In a Multi-City Case-Only Analysis. *Epidemiology (Cambridge, Mass.)*, 24 (6):809–819, November 2013. ISSN 1044-3983. doi: 10.1097/01.ede.0000434432.06765.91. URL <https://www.ncbi.nlm.nih.gov/pmc/articles/PMC4304207/>.